

ABSTRACT

Title of Document: GENETIC CHARACTERIZATION OF TOXIC HEME RESISTANT MUTANTS IN *C. elegans*

Jonathan Walston, Masters of Science, 2010

Directed By: Associate professor Dr. Iqbal Hamza, Department of Animal and Avian sciences

Heme is an essential cofactor that plays a key role in diverse biological processes. Free heme, however, is hydrophobic and toxic to cellular macromolecules. *C. elegans* lack the heme biosynthetic pathway, and therefore contains a highly regulated trafficking network to redistribute heme throughout the worm. A forward genetic screen in *C. elegans* identified thirteen mutants which grow at toxic concentrations of heme in axenic liquid media. These mutants, termed *them* for Toxic HEMe resistant, belong to five complementation groups of which IQ7280, IQ7310, IQ8280 and IQ9110 strains were characterized. *them* mutants exhibit abnormal responses to heme analogs, mating defects, and growth on heme-deficient bacteria. Pyrosequencing analysis mapped IQ7310, IQ8280, and IQ7280 to a common genetic interval on chromosome I and IQ9110 to chromosome V. Solexa deep sequencing identified mutations in novel genes which may play an essential role in organismal heme homeostasis.

GENETIC CHARACTERIZATION OF TOXIC HEME
RESISTANT MUTANTS IN *C. elegans*

By
Jonathan Walston

Thesis submitted to the Faculty of the Graduate School of the
University of Maryland, College Park, in partial fulfillment
of the requirements for the degree of
Masters of Science
2010

Advisory Committee:

Dr. Iqbal Hamza, Chair
Dr. David Eisenmann
Dr. Lisa Taneyhill

© Copyright by
Jonathan Walston
2010

Dedication

To my father, Dennis C. Walston, who I miss dearly.

I wish you could see how far I have come.

Acknowledgements

Thank you to my advisor Iqbal who has not only helped develop my critical thinking of the biological sciences, but has also aided my efforts in becoming a veterinarian. I would never have been able to get this far without his encouragement, of which I am deeply appreciative.

To Scott and Anita, thank you for mentoring me at the bench and through the process of completing my Masters. Scott, thank you especially for helping me develop my scientific writing skills, without which I would not have been able to complete this thesis.

To Dr. Harold Smith, thank you for sequencing the entire genome of *them* mutants which allowed me to make forward progress on my project when it seemed stagnant.

To Jason, thank you for microinjecting my rescue constructs of which I would not have been able to complete this project. I have not only appreciated your technical abilities, but also your friendship since I first joined the lab.

To the Hamza lab, past and present members I am thankful for the guidance, friendship and support you have all given me over the past two years.

Lastly, to Mom, Erika, Hanna, and Nicole, you have all supported me throughout my Masters, and still support me now. You have helped me stand strong when work seemed overwhelming. For this, I can never be grateful enough.

Table of Contents

Dedication.....	ii
Acknowledgements.....	iii
Table of contents.....	iv
List of Tables.....	vi
List of Figures.....	vii
Chapter 1. Literature review.....	1
Introduction.....	1
Heme biosynthesis.....	3
Transcriptional regulation by heme.....	10
Heme transporters.....	12
<i>Caenorhabditis elegans</i> as an animal model.....	15
Parasitic helminths.....	18
Next generation sequencing.....	20
Chapter 2. Methods.....	25
<i>C. elegans</i> growth media.....	25
Strains.....	25
Synchronization of <i>C. elegans</i>	26
Preparation of hemin chloride.....	26
Zinc mesoporphyrin.....	27
Gallium protoporphyrin IX toxicity assay.....	27
Cloning of RNAi constructs.....	28
Brood size assay on <i>hemB</i> bacteria.....	29
Male production.....	29
Mating efficiency assay.....	30
Pyrosequencing.....	30
Two-factor recombination mapping.....	32
Deficiency mapping.....	33
Sanger DNA sequencing.....	33
Genome sequencing.....	33
Microinjection of rescue construct.....	34
Toxic heme resistance rescue experiment.....	35
Chapter 3. Results.....	36
A forward genetic screen to identify toxic heme resistant mutants.....	36
Genetic mapping by pyrosequencing identifies the genomic locus for <i>them</i> mutations.....	37
Two-factor and deficiency mapping confirms pyrosequencing.....	40
Gallium protoporphyrin IX RNA interference screen identifies <i>them</i> candidate genes within the mapped genetic interval.....	42
Further characterization of <i>them</i> phenotypes.....	44
Whole genome sequencing to identify <i>them</i> mutations.....	47
Chapter 4. Discussion.....	79
Appendices	
Appendix A: Toxic heme resistance mutagenesis screen design.....	89
Appendix B: Heme dependent growth curves of <i>them</i> and resulting phenotypic clusters.....	91

Appendix C: List of thirteen <i>them</i> strains organized into five complementation groups and three phenotypic clusters.....	93
Appendix D: List of primers used in pyrosequencing.....	94
Appendix E: <i>them</i> mutant worms exhibit GaPP resistance in mCeHR-2 liquid media.....	97
Appendix F: List of primers used to clone missing constructs for GaPP RNAi screen.....	99
Appendix G: List of primers used to confirm mutations in <i>them</i> genomes.....	101
References.....	103

List of Tables

Table 1. List of SNP markers and the N2 percentage for <i>them</i> mutants on each of the six chromosomes.....	70
Table 2. List of SNP markers and the N2 percentage for <i>them</i> mutants for <i>them</i> mutants along chromosome I and V.....	72
Table 3. Two-factor recombination map and deficiency map of <i>them</i>	74
Table 4. List of genes analyzed in the GaPP RNAi screen.....	76
Table 5. List of candidate genes from the GaPP screen with descriptions.....	77
Table 6. Candidate genes with mutations identified through Solexa deep sequencing.....	78

List of Figures

Chapter 1

Figure 1. Heme biosynthesis in eukaryotes..... 5

Chapter 3

Figure 1. A visualization of SNP and mutant alleles used in mapping
for chromosome I and V..... 52

Figure 2. *them* mutants exhibit GaPP resistance..... 54

Figure 3. GaPP resistance screened in candidate genes for *them*..... 56

Figure 4. ZnMP uptake is reduced in *them*..... 58

Figure 5. *them* brood size is dependent upon nutrient levels derived
from bacteria..... 61

Figure 6. *them* mutants exhibit a male mating deficiency..... 63

Figure 7. Reduced ZnMP uptake exhibited by *C. elegans* exposed to
RNAi of candidate genes..... 65

Figure 8. Rescue of *them* phenotype by microinjection of wild-type *nhr-147*
in IQ9110..... 68

Chapter 4

Figure 1. Homologous amino acid sequence between *nhr-147* and *nhr-149*..... 87

Chapter 1: Literature Review

Introduction

Iron is an essential micronutrient for nearly all living organisms. The reason it is so vital stems from its ability to be reduced (Fe^{+2}) and oxidized (Fe^{+3}), permitting the function of a number of proteins involved in oxidation and reduction reactions. However, iron must be tightly regulated since this oxidative attribute allows it to catalyze the production of free radicals, which have been linked to a range of disorders including cancer, arthritis, atherosclerosis, Alzheimer's disease, and diabetes (1).

Even though iron is an abundant element throughout the planet, its bioavailability is scarce. Therefore, it is not surprising that iron deficiency is a common problem, causing greater than thirty percent of the global population to suffer from anemia (2). A major issue of iron absorption in humans is that inorganic iron is insoluble at duodenal pH, which ranges from 5-7 (3). Moreover, since plant matter makes up the majority of human diet worldwide, the presence of chelators such as phytates in plants makes iron inaccessible for absorption (4). A readily bioavailable source of iron is heme (iron protoporphyrin IX), which is present in most red meat, and is absorbed through the intestine (5,6); the factors that negatively affect Fe absorption do not affect heme absorption. However, little is known about how heme is absorbed and trafficked through intestinal cells.

Heme consists of a tetrapyrrole ring with an iron atom residing in the center (7). Heme is a required cofactor for a variety of proteins such as transcription factors, globins, cytochromes, and catalases (8). This allows heme to participate in a wide array of

biological processes including oxygen transport, electron transport, xenobiotic detoxification, signal transduction, circadian clock control, and microRNA processing (9).

Heme biosynthesis has been thoroughly studied (10). Most eukaryotic organisms synthesize heme through a conserved eight-step pathway which is catalyzed in both the mitochondria and the cytosol (7). The enzymes have been crystallized and characterized in great detail (11). In contrast to the well-understood biosynthetic pathway, the trafficking network that transports heme to be incorporated into various compartments and proteins is relatively unexplored. As a result of heme containing an iron atom, it has the ability to create free radicals. Consequently, tight regulation over the movement of heme by directed transport and possible chaperoning of heme to its target compartments are essential to prevent heme's cytotoxic effects (12).

Elucidating the network of heme trafficking pathway is difficult because it requires the separation of heme synthesis from trafficking which are normally intrinsically linked. Genetic depletion of heme through mutations within the heme biosynthesis pathway causes pleiotropic phenotypes and lethality (13). Our research group has shown that *Caenorhabditis elegans* (*C. elegans*) lack the entire heme biosynthesis pathway naturally and depend on exogenous heme for survival (14). Thus, *C. elegans* is a tractable animal model to identify the genes responsible for heme transport and its impact on organismal growth and development.

In addition to *C. elegans*, a number of related parasitic helminths lack the heme biosynthesis pathway (14). Parasitic worms place an enormous economic burden on

agriculture and human health (15,16). Over two billion people worldwide are infected by parasitic helminths (16). The treatment of helminthic infections is complicated by emerging resistance of the parasites to commonly used anthelmintics (17). Since these parasites lack the heme biosynthesis pathway, they must obtain heme from their host in order to have functional hemoproteins. This suggests that they may contain unique genes to maintain heme homeostasis. These unique genes would be helminthic-specific, thereby providing novel potential drug targets.

Identification of novel genes through mutagenesis screens is a productive approach to identify novel gene function; however, mapping these mutations is time-consuming. The use of recombination and restriction fragment length polymorphism mapping can take months and even years to pinpoint the mutation causing a phenotype of interest. Fortunately, with next generation sequencing, whole mutant genomes can be sequenced in a matter of days, allowing the identification of mutations to be a rapid process (18). This burgeoning technology has the potential to change the way classic mutation mapping has been performed in the past.

Heme Biosynthesis

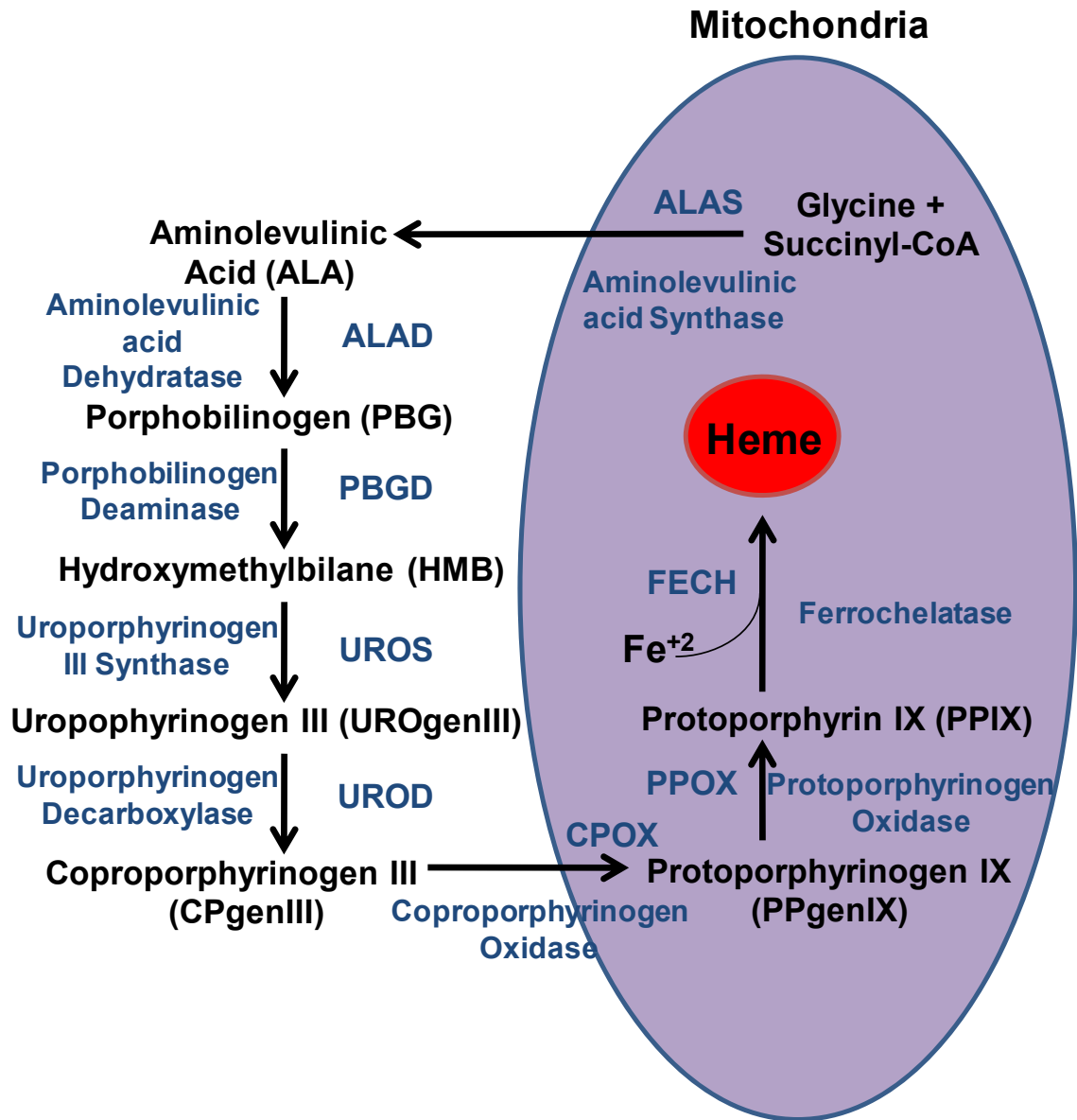
In most eukaryotic and some prokaryotic organisms, heme is synthesized through a highly conserved eight step pathway known as the Shemin pathway (19). In metazoans, the first and last three steps occur in the mitochondria, while the other four intermediate steps take place in the cytosol (Fig. 1A). All eight of the heme biosynthesis enzymes have been well characterized as each has been cloned and crystallized (11).

In all metazoans, heme biosynthesis begins with the synthesis of δ -aminolevulinic acid (ALA) through the condensation of glycine and succinyl-CoA (19). This reaction is catalyzed by aminolevulinic acid synthase (ALAS), an enzyme that is encoded by two different genes (20): *ALAS1* is expressed in all tissue types and the gene is present on chromosome III and *ALAS2* is present on the X chromosome and is expressed only in erythroid cells. *ALAS1* and *ALAS2* are differentially regulated at the transcriptional level. *ALAS1* is regulated by the transcription factor NPAS2, which is important for regulating the circadian clock (21). A heterodimeric complex of NPAS2 and BMAL1, a aryl hydrocarbon receptor nuclear translocator, binds the *ALAS1* promoter to enhance transcription. However, the binding of heme to NPAS2 prevents the heterodimer formation and causes the repression of *ALAS1* gene transcription (21). *ALAS2* has erythroid specific expression because it is transcriptionally regulated by the erythroid specific transcription factor GATA1. GATA1 and histone acetyltransferase p300 interact to induce the *ALAS2* promoter (22). The mature ALAS enzyme is expressed in the mitochondrial matrix, and requires a cofactor, the active form of vitamin B₆, pyridoxal 5-phosphate, to function properly (8). ALA is thus synthesized within the mitochondrial matrix, and is transported to the cytosol by an unknown transporter.

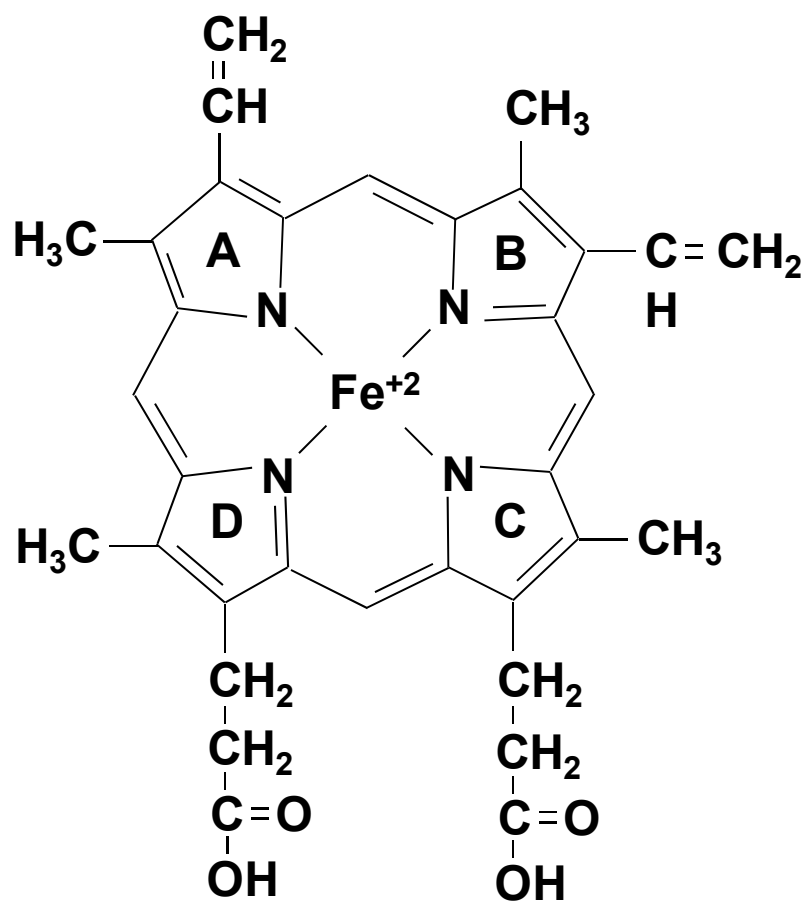
Figure 1. Heme biosynthesis in eukaryotes

A) Heme biosynthesis is an eight step pathway that occurs within the mitochondria and cytosol. It begins with the synthesis of aminolevulinic acid by ALAS in the mitochondria. The next four steps occur in the cytosol, ending with the intermediate product coproporphyrinogen III. This compound is transported back into the mitochondria for the final three steps of the heme biosynthesis pathway. The intermediate products are labeled in black and the enzymes are labeled in blue. B) The structure and chemical composition of heme B. Each of the pyrroles are labeled A-D.

A



B



Following its transport to the cytosol, two ALA molecules are grouped to create PBG by aminolevulinic acid dehydratase (ALAD) which creates porphobilinogen (PBG) through a condensation reaction. PBG synthesis is dependent on zinc availability as this metal acts as a cofactor to the ALAD enzyme (23). The functional ALAD enzyme is a complex composed of four homodimers, with each homodimer containing an active site that binds two ALA molecules (24). One of the ALA molecules is used to synthesize the propionate side chain and pyrrole nitrogen, while the other ALA molecule creates the acetate and amino-methyl group of PBG (25). PBG provides the foundational pyrrole in all living organisms for the creation of many different types of tetrapyrroles, including heme (26).

The next two enzymes in the pathway work together to create the important asymmetric side chains of the porphyrin ring – these side chains allow its insertion into various hemoproteins and is essential for heme's physiological role. The first enzyme, porphobilinogen deaminase (PBGD), polymerizes four PBG molecules to synthesize the linear tetrapyrrole, hydroxymethyl bilane (HMB). This molecule is released from PBGD after the four pyrroles distal to the active site are cleaved. This results in PBGD retaining the two proximal pyrroles to be used in subsequent reactions as a dipyrrole cofactor (27).

Once HMB has been released by PBGD, it is not stable enough to retain its structure and if not quickly utilized as substrate will form uroporphyrinogen I. This is a tetrapyrrole that cannot be converted to heme, therefore the next enzyme in the pathway, uroporphyrinogen III synthase (UROS), has to catalyze pre-uroporphyrinogen into uroporphyrinogen III (UROgenIII) rapidly, or the isoform uroporphyrinogen I will be

synthesized. UROS does so by closing the linear pre-uroporphyrinogen into a ring which changes the substrate to a asymmetrical macrocycle (8).

In the last step to occur within the cytosol of metazoans, UROgenIII is converted to coproporphyrinogen III (CPgenIII) by the enzyme uroporphyrinogen decarboxylase (UROD). UROD catalyzes the removal of carboxylic acid groups from the four acetic acid side chains of UrogenIII. This heme precursor is then transported back to the inner membrane space of the mitochondria where further modification of the tetrapyrrole side chains occurs. The transport of UrogenIII has been proposed to be carried out by the protein ABCB6 in mammals (28). However, this claim has been disputed since ABCB6 has been found to localize to the plasma membrane, Golgi, as well as the inner membrane space of the mitochondria (29,30). Its efficiency as a porphyrin transporter has also been questioned since the studies used coproporphyrin III, a non-physiological, planar, oxidized molecule instead of the physiological non-planar reduced CPgenIII (28). Regardless of whether or not ABCB6 is the transporter, CPgenIII must find its way into the inner membrane space of the mitochondria for heme biosynthesis to continue.

Coproporphyrinogen oxidase (CPOX) is the sixth enzyme in the heme biosynthesis pathway. This enzyme is localized to the mitochondrial outer membrane with the active site oriented towards the inner mitochondrial space (31). CPOX utilizes CPgenIII as a substrate and converts the propionate side chains of pyrroles A and B in to vinyl groups (Fig. 1B). This oxidative decarboxylation reaction converts CPgenIII to protoporphyrinogen IX (PPgenIX). CPOX is the rate limiting enzyme for heme biosynthesis during erythroid differentiation (32).

PPgenIX is converted to protoporphyrin IX (PPIX) by the enzyme protoporphyrinogen oxidase (PPOX), which is located on the mitochondrial inner membrane facing towards the inner membrane space (33). PPOX performs a six-electron oxidation of PPgenIX, a flexible molecule, to generate PPIX, a rigid planar ring.

The last step in heme biosynthesis is catalyzed by ferrochelatase (FECH), the enzyme responsible for inserting the iron atom into the center of the PPIX molecule. FECH is located on the matrix side of the inner membrane of the mitochondria. As a result of the active site of FECH facing the inner membrane, protoheme is released toward the membrane instead of the matrix (7). Once heme has been synthesized it will be incorporated into various hemoproteins as a cofactor. While it plays a functional role as a cofactor, it also has the ability to transcriptionally regulate gene expression (34).

Transcriptional Regulation by Heme

Heme has been shown to be involved in the transcriptional regulation of various genes. Cellular functions such as circadian clock control and oxidative respiration have been shown to be dependent on intracellular heme levels (34,35).

Evidence of heme's role as a transcriptional regulator in *C. elegans* has been identified through a DNA microarray (36). As a result of *C. elegans* being grown in three different concentrations of heme, 370 genes were identified to be transcriptionally regulated by heme (36). These genes were termed *heme responsive genes (hrgs)* and were organized into eight different categories. These categories were created based upon the *hrgs* transcriptional profile under three different heme concentrations (36). Transcriptional regulation by heme has also been shown in mammalian cells. A DNA

microarray was conducted in K562 cells which were treated with heme a single concentration of heme (37). From this microarray, several hundred genes were identified to be upregulated or downregulated in the presence of heme, which indicates heme has the ability to activate and repress gene transcription (37). Heme has been demonstrated to play a role in the transcriptional regulation of genes involved in circadian clock control. The nuclear hormone receptor REV-ERB α has been shown to bind heme, which allows it to recruit its binding partner, NCoR-HDAC3 (34). Experimental evidence shows that this complex downregulates various gluconeogenic genes which are involved in circadian rhythm (38).

An essential role of heme in mammals is its function in respiration. Heme is the cofactor in hemoglobin responsible for binding oxygen. Additionally, heme also has the ability to transcriptionally regulate hemoglobin production. Hemoglobin in mammals is produced in erythroid tissue. The structure of hemoglobin consists of four subunits, two α -globin chains and two β -globin chains which form a heterotetramer. Each subunit contains a heme molecule, which allows a single hemoglobin molecule to bind four oxygen atoms (39). Under low heme conditions, the production of globin chains is downregulated given that aggregation of globin chains is toxic to the cell (40). Globin chain production has been shown to be transcriptionally regulated by Bach1. Bach1 regulates globin chain production through a locus control region (LCR) (41). The LCR is approximately 60 kb from five genes which encode ϵ -globin, G γ -globin, A γ -globin, β -globin, and δ -globin proteins. Bach1 is able to control the transcription of each of these genes by binding to MARE sequences (Maf Recognition Element) which is located within the LCR. The MARE sequence recruits Maf proteins which activate and repress

gene expression depending on with which transcription factor it dimerizes (42). Under low heme conditions, Bach1 dimerizes with Maf, binds to the MARE sequence and repress transcription of globin chains. However, once sufficient heme is produced in the cell, heme binds Bach1 and the Bach1/Maf complex dissociates from the MARE sequence, allowing transcriptional activation of the globin chains (41). Through Bach1, intracellular heme concentrations are able to dictate transcription of globins, thereby the production of hemoglobin.

Heme Transporters

While the heme biosynthesis pathway has been extensively researched, there is relatively little known about the trafficking network that delivers heme to hemoproteins around the cell. Proteins such as hemoglobin, myoglobin, cytochromes, Bach1, REV-ERB α , catalases and peroxidases all require heme to function properly. As a result of heme's cytotoxic reactivity, heme trafficking must be tightly regulated in accordance with cellular requirements.

The first metazoan heme importer discovered was *heme responsive gene 1* (*hrg-1*). This gene was initially discovered through a microarray identifying genes in *C. elegans* that respond to different concentrations of environmental heme. Worms grown in liquid culture supplemented with 4 μ M heme showed >10-fold upregulation of *hrg-1*. HRG-1 is a 194 amino acid protein with four transmembrane domains and is the only member of the solute carrier family 48 (Slc48a1). While in *C. elegans* there exist four paralogs of *hrg-1*, humans only contain one homolog (36).

Localization studies in HEK293 cells have shown that both the worm and human HRG-1 colocalize to the late endosomal and lysosomal compartments. Furthermore, *Xenopus* oocytes expressing *hrg-1* revealed electrophysiological currents in the presence of heme, indicating the transport of heme across membranes (36).

Genetic studies have examined the importance of *hrg-1* in embryonic development using morpholino knockdown of zebrafish *hrg-1*. *hrg-1* knockdown in zebrafish embryos results in severe anemia, hydrocephalus and a curved body with shortened yolk tube. All of these phenotypes are completely rescued with *C. elegans* *hrg-1* which is only ~20% identical to zebrafish *hrg-1* at the amino acid level. These results emphasize the importance of keeping this particular heme transporter functionally conserved, even if these proteins have diverged at the amino acid level (36).

Another heme transporter which is nematode specific is a paralogue of *hrg-1*: *heme responsive gene 4 (hrg-4)*. Studies using microarray analysis, RNA blotting, and qRT-PCR show that the gene is upregulated >40 fold upregulated at 4 μ M heme and undetectable at concentrations as low as 20 μ M heme. The HRG-4 protein is 207 amino acids in length, containing four predicted transmembrane domain and when expressed in HEK293 cells, HRG-4 localizes to the plasma membrane. Transport studies in *Xenopus* oocytes showed a greater transport activity of heme for *hrg-4* than that seen for *hrg-1* (36).

In *C. elegans*, both *hrg-1* and *hrg-4* are intestinal-specific genes. HRG-4 is proposed to function as the intestinal heme importer in the worm intestine. This is supported by its ability to transport heme and its localization to the apical membrane of the intestinal cell. On the other hand, HRG-1 localizes to the late endosomal and

lysosomal compartments and is expressed under low concentrations of heme, suggesting that HRG-1 may transport heme from these compartments into the cytosol when intestinal intracellular levels of heme are low (36).

Two other heme exporters have been reported in red blood cells (RBCs): the feline leukemia virus subgroup C receptor (FLVCR) and the ATP-binding cassette, subfamily G, member 2 (ABCG2). FLVCR was first identified as a cell surface receptor for the feline leukemia virus subgroup C (43). Cats infected with this virus show symptoms of aplastic anemia. The glycoprotein region 1 of the viruses surface envelope was found to bind to FLVCR which then internalizes the virus (44,45). Symptoms of infection result from the failure of erythroid progenitor cells to mature from the burst forming unit to the colony forming unit, thus halting cell differentiation and resulting in anemia (46). *FLVCR* shows tissue expression in hematopoietic cells, and is weakly expressed in the fetal liver, pancreas, and kidney (46). FLVCR has been shown to mediate the efflux of the fluorescent heme analog zinc mesoporphyrin in rat renal epithelial and hematopoietic K562 cells, and this FLVCR-mediated heme efflux is proposed to be important for erythroid cell differentiation (47). The role for FLVCR in erythroid differentiation is supported by a study in which knockout of *FLVCR* in mice results in the failure of erythroid differentiation and causes death at midgestation. These mice also exhibit cranio-facial and limb deformities that resemble the symptoms of patients with the severe but rare congenital erythroid anemia, Diamond-Blackfan anemia.(48)

ABCG2 is another putative heme transporter in RBCs. This protein was initially discovered as breast cancer resistance protein (BCRP) that causes drug resistance in breast cancer cells (49). The first evidence for a potential role for ABCG2 in heme

transport came from *ABCG2* knockout mice that were fed a modified diet and exhibited skin photosensitivity, a common symptom of porphyrias (50). Porphyrias occur when there is an overproduction and accumulation of the chemical precursors of the heme biosynthetic pathway. Further examination of this phenotype showed that the photosensitivity was due to the accumulation of pheophorbide A, which is a degradation product of chlorophyll and is similar in structure to PPIX (51). As a result of these phenotypes, it was found to play a role in the exportation of xenobiotic toxins.

While there are most likely a number of proteins involved in heme transport, identifying them has been a difficult task. However, two of the four transporters identified in metazoans have been discovered using the animal model *Caenorhabditis elegans*. As such, *C.elegans* provides a powerful model system that is genetically tractable and devoid of endogenous heme synthesis in order to identify the components of heme homeostasis and regulation within the context of a whole animal.

***Caenorhabditis elegans* as a model organism**

Caenorhabditis elegans has been an established animal model since the 1960s (52). It contains a number of attributes which make it an excellent model to study many biological questions. *C. elegans* was the first multicellular organism to have its entire genome sequenced and shows strong conservation with mammals in a variety of molecular and cellular pathways (53). Approximately 42% of predicted protein products show conservation with proteins outside the phylum Nematoda (53). Some of these conserved proteins are orthologous to human proteins which are linked to diseases such as Alzheimer's disease, Parkinson's disease, muscular dystrophy, and polycystic kidney

disease (54). The hermaphrodite contains 959 somatic cells and many different organs and tissues including muscle, hypodermis, intestine, reproductive system, and a nervous system. In place of blood it has a pseudocoelomic fluid which suspends the intestine and gonads within the body cavity. Each of the 959 cell lineages in *C. elegans* has been carefully mapped, providing a tractable tool for studying development. *C. elegans* is easy to culture in large quantities, either in axenic liquid media CeHR-2 or on agar plates seeded with a lawn of bacteria, one of *C. elegans*'s natural food sources. In addition, *C. elegans* develops from the larval stage to an egg laying adult in 3.5 days and is 1.3 mm in length. Its size and rapid generation time allows it to be grown in a small space such as a 96-well plate over a short period of time, which makes high throughput screens more manageable (55).

Another benefit to genetic studies is that the organism is hermaphroditic, with each hermaphrodite producing approximately 300 progeny. Hermaphrodites essentially create clones of themselves, allowing easy propagation of homozygous mutant lines. Males are created through an X chromosomal nondisjunction which occurs naturally in every one out of 500 progeny. The sperm from males preferentially fertilizes the eggs of hermaphrodites, allowing for genetic crosses to be carried out (55).

Since these organisms can be screened in large populations, they are very tractable for forward genetic screens. *C. elegans* can be mutagenized by being exposed to radiation, X-rays or chemicals such as ethylsulfonic acid (56). These animals can then be screened for a phenotype of interest, characterized, and the genetic lesion must then be mapped. There are a number of useful genetic tools available to *C. elegans* researchers.

The Caenorhabditis Genetics Center which is located at the University of Minnesota provides strains for mapping as well as characterization.

Another useful characteristic is that the organism is transparent. This means that fluorescent markers can be used to look at a variety of process such as nutrient uptake, axonal growth, embryogenesis and gene regulation in a live animal. For example, our lab has examined the regulation of *hrg-1* by heme using a transcriptional green fluorescent protein (GFP) reporter. This construct was microinjected into *C. elegans* to create a transgenic strain. When this strain of *C.elegans* was placed in low heme, each of the organisms' upregulated GFP expression, if an individual from that population is then placed in high heme the GFP is downregulated and expression can no longer be detected. If this same animal is placed back into low heme then GFP expression is observed again, showing the heme-dependent regulation of the *hrg-1* gene in a single animal (36).

The most essential physiological aspect of *C. elegans* for our research group is that it lacks all eight steps in the heme biosynthesis pathway (14). The greatest problem with identifying new molecules and pathways involved in heme homeostasis has been the inability to dissociate the tightly controlled heme biosynthesis pathway with intracellular trafficking. The heme biosynthetic pathway has been knocked down in other model organisms; however, it still becomes difficult to identify novel proteins involved in heme trafficking since they lack the appropriate machinery to obtain heme from another source besides the mitochondria. Since *C.elegans* lacks the heme biosynthesis pathway, this presents the opportunity to study heme trafficking without the complication of endogenous heme. When *C. elegans* is grown in liquid axenic growth media mCeHR-2 in varying concentrations of heme, they present a biphasic growth curve, relying on

exogenous heme from the environment for normal growth and reproduction (14). In liquid, *C. elegans* can grow in mCeHR-2 media with supplemented heme concentrations ranging from 1.5 μM to less than 800 μM . Furthermore, these animals contain genes which encode for a large number hemoprotein orthologs such as guanylate cyclases, adenylate cyclases, globin isoforms, and cytochrome P450s (57-60). Therefore, it is theorized that they must contain a sophisticated heme storage and intracellular transport system to provide these proteins with heme and to maintain heme homeostasis in all cells.

Parasitic Helminths

C. elegans is phylogenetically related to a number of helminths which makes it a relevant model for these types of parasitic nematodes. Many of these parasites have also been found to be heme auxotrophs, lacking the enzymatic activity of the enzymes within the heme biosynthesis pathway (14). Some of these helminths are *Strongyloides stercoralis*, *Ancylostoma caninum*, *Haemonchus contortus*, *Trichuris suis* and *Ascaris suum*. Since these parasites feed off the blood of their hosts, they are engorged with heme from hemoglobin, which means they need to not only take up this heme for their own metabolic processes, but they also need to possess the ability to manage such high concentrations of a cytotoxic compound.

Helminthic infections place a large economic burden on both agriculture and human health. It has been reported that over two billion people globally are infected with at least one type of helminth, and global agricultural economic losses from plant parasitic nematodes is estimated at 125 billion dollars annually (15,61). Finding new ways to combat these parasites is essential since they are quickly becoming more resistant to the

commonly used anthelmintics (17). One way to develop new anthelmintic drugs would be to target nematode specific proteins. Since many of the helminths lack the heme biosynthesis pathway, heme uptake provides an appealing area to locate nematode-specific targets.

It has been suggested that there is a direct link between host diet and severity of the helminthic infection (62). Hookworm infections due to *Ancylostoma ceylanicum* are quite prevalent in developing countries. Individuals infected with hookworms show symptoms that are linked with inflammation of the gut such as diarrhea, abdominal pain, and in severe infections, anemia. One study has demonstrated how the host's iron status affects the hookworm pathogenicity (62). In this study the research group utilized hamsters which were infected with hookworms and fed them either a normal diet or a diet which was deficient in iron. Animals fed a diet in which iron was restricted showed a significant reduction in the number of intestinal hookworms when compared to animals fed a nutritionally sufficient diet (62). This suggested that the hookworms are sensitive to the iron deficiency in the animal and require host iron for normal growth and reproduction. It is common practice to give iron supplements alongside anthelmintics to individuals infected with hookworms since they tend to be anemic. However, this treatment may exacerbate the parasitic infection, making it more difficult for the anthelmintics to work.

A different parasitic species has been able to find a symbiotic method to bypass the need for the heme biosynthesis pathway. The filarial nematode *Brugia malayi* is the parasitic helminth that is responsible for lymphatic filariasis, also known as elephantitis, which is prevalent in tropical areas. An analysis of the *B. malayi* genome found that all

the enzymes in the heme biosynthetic pathway, except for ferrochelatase, are missing (63). *B. malayi* contains many hemoproteins that are present in all eukaryotic organisms, so the parasite must absorb its heme either from its human host or through its symbiont, the intracellular bacterium, *Wolbachia*. *Wolbachia*, unlike *B. malayi*, has all of the enzymes necessary for heme biosynthesis except for one, PPOX (63). It also appears that *Wolbachia* is essential for the survival of *B. malayi*. One study in which antibiotics were used to deplete endogenous *Wolbachia* from *B. malayi* have shown that this caused the adult worms to die (64). This means that the *Wolbachia* must be providing *B. malayi* some benefit, which could possibly be heme or some other metabolite which is essential for *B. malayi*'s survival. The proteins by which heme is transferred between *Wolbachia* and its host could be examined as possible drug targets for future anthelmintics.

The ability to compare genomes between parasitic helminths and *C. elegans* has been important for establishing the deficiencies within the heme biosynthetic pathway of these parasites (14). With advancement in sequencing techniques, whole genomes of many different organisms are being analyzed at an exponential pace providing new insights into these organisms' metabolic structure.

Next Generation Sequencing

The field of DNA sequencing has made incredible progress in the last decade. While it originally took years to sequence an entire genome, it now takes weeks. Now that many model organisms have had their entire genomes mapped and annotated, this provides a reference to align the short reads that are used in second generation

sequencing (53,65). This advancement in technology has made it possible to sequence the entire genome of mutant organisms instead of using conventional genetic mapping to find the mutation. All of these advancements have been a result of cost reduction in conventional sequencing through an optimization of these techniques.

Conventional or first generation DNA sequencing is performed through the use of capillary-based semi-automated implementations of the Sanger biochemistry (66,67). DNA using Sanger sequencing is prepared by two methods. The first method, which is commonly referred to as shotgun *de novo* sequencing, is to randomly fragment the genomic DNA and clone it into a high-copy-number plasmid, which would then be transformed into *E. coli* for replication. The second method for preparation is used for targeted resequencing. This employs PCR amplification of a particular fragment using primers specific to the region of interest. The sequencing takes place in cycling reactions in which template denaturation, primer annealing and primer extension are performed. During each round of sequencing, primer extension can be terminated if the fluorescently tagged dideoxynucleotide (ddNTPs) is added to the strand. This provides a mixture of different length fragments with a variety of terminating nucleotides. The sequence is then read by high-resolution electrophoretic separation of the single-stranded DNA products in a capillary based polymer gel. The fluorescent labels are then excited by a laser as they exit the capillary and are read by four color detection emission spectra. These spectra are then analyzed by software and generate a sequence depending on the fluorescence and length of the fragment. Average reads presently produce maximum lengths of up to 1000 base pairs (68).

The second generation sequencing methods can be organized into four categories. These are microelectrophoretic methods (69), sequencing by hybridization (70), real-time observation of single molecules (71) and cyclic array sequencing (72). While each of these methods use very different sequencing biochemistry, they follow very similar steps in DNA preparation. The first step is to create a library which is done by random fragmentation of DNA followed by ligation of common adaptor sequences. Then these fragments are amplified by either *in situ* polonies (polymerase colonies), emulsion PCR or bridge PCR (73). Each of these methods are similar since they start with a single strand of DNA and end up with a spatial cluster of copies of that sequence. The sequencing process of all of these methods involves alternating cycles of enzyme-driven biochemistry and imaging-based data collection (18).

One of the more common next generation sequencing methods is the Solexa platform which uses cyclic array sequencing in which adapter flanked fragment libraries of about 200 base pairs in length that are tethered to a solid substrate by a flexible linker to keep strands in place during amplification. Each of these sequences is amplified by bridge PCR which uses alternates cycles of extension with *Bacillus stearothermophilus* (*Bst*) polymerase and denaturation with formamide (73). Each of these sequences form clonal amplicon clusters that consist of about 1000 copies. After the amplification process, the strands are linearized, a universal primer binds to the adapter, and reversible terminators are added. These reversible terminator nucleotides have a chemically cleavable moiety at the 3' hydroxyl position which allows only one nucleotide to be added during one cycle. Each of these reversible terminators also contains a different fluorescent tag, corresponding with each of the four nucleotides, which can be chemically

removed (74). During each cycle an image is taken and each of the different color fluorescence clusters is recorded as a specific nucleotide. This method produces read lengths of up to 36 base pairs. The average error rate is from 1-1.5%, but accuracy can be improved using higher fold coverage of the genome (18).

While sequencing the entire genome is useful, the process of finding the mutation is very tedious since single nucleotide polymorphisms (SNPs) occur frequently throughout the genome. One way to narrow down possible mutations is to use second generation sequencing to perform recombination mapping (65). A mutant line can be crossed to a mapping strain with recognized unique SNPs. Utilizing 454 pyrosequencing platform, the percentage of SNPs transferred through recombination can actually be quantified. Pyrosequencing works by emulsion PCR, where strands of a similar sequence become tethered to streptaovidin beads and go through rounds of amplification with *Bst* polymerase. Once each bead is saturated with copies of the template double-stranded DNA, it is treated with a denaturant and washed to remove the strand of the DNA which is not tethered to the bead. The beads are then placed in a special plate which contains individual picoliter scale wells where the beads settle. A primer designed to be specific for the region containing the SNP is used to allow the *Bst* to add individual nucleotides. The 454 machine records the nucleotide being added and whether or not it is incorporated through a biochemical reaction involving ATP sulfurylase and luciferase to produce light (18). In this way, entire recombination maps can be made from individual recombinant organisms (65). This allows possible candidate genes to be narrowed down to a more reasonable number when the entire genome is sequenced.

Not only will mutations be easier to map, but next generation sequencing also provides the ability to find mutations which were once thought impossible to map. *C. elegans* already has an impressive track record for its contributions to our understanding of biology; however, since it is a natural heme auxotroph, it has and will play a critical role in elucidating the genetic pathway for heme trafficking. With proteins involved in heme homeostasis being identified, similarities between parasitic species and *C. elegans* provides the opportunity to locate new and powerful drug targets to stop the spread of helminthic infections.

Chapter 2: Materials and Methods

C. elegans growth media

C. elegans strains worms were cultured in axenic mCeHR-2 liquid medium supplemented with varying concentrations of hemin while being shaken at 20°C (75) or on nematode growth medium (NGM) plates containing 3 g/L NaCl, 2.5 g/L peptone, 30 g/L agar, 5 mg/L cholesterol, 1 mM MgSO₄, 1 mM CaCl₂, and 25 mM KH₂PO₄. Plates were spotted with *E. coli* strain OP50 as a food source for the worms. NGM plates used in RNA-mediated interference (RNAi) plates were supplemented with 50 µg/mL carbenicillin, 12 µg/mL tetracycline, and 2 mM IPTG and seeded with HT115(*DE3*) *E. coli*. HT115(*DE3*) bacterial cultures were inoculated in Luria-Bertani broth containing 50 µg/mL carbenicillin and 12 µg/mL tetracycline (LB+carb+tet) and were incubated at 37°C shaking at 260 rpm overnight. The following day, the overnight culture was used to inoculate fresh LB+carb+tet using a 1:12 ratio of overnight culture to fresh LB+carb+tet. This culture was incubated at 37°C rotating at 260 rpm for 5.5 h and then seeded on the RNAi agar plates.

Strains

Wild-type *C. elegans* N2 Bristol strain was used in all experiments. The following *C. elegans* strains were used in mapping experiments: CB4856 (HA), CB713 (*unc-70*), CB524 (*unc-67*), BC1283 (*eT1/sDf20*). All strains were maintained on NGM plates seeded with OP50 and incubated at 20°C with the exception of *C. elegans* strain BA17 (*fem-1*) which was used to assay mating deficiency. This strain was maintained on NGM plates seeded with OP50 and incubated at 25°C. Additionally, *C. elegans* strain VC1585

(*nhr-147*) was used for rescue experiments and maintained at 20°C. All strains were obtained from The Caenorhabditis Genetics Center (University of Minnesota, MN).

Synchronization of *C. elegans*

Worms grown in mCeHR-2 were centrifuged at 800 x g for 5 min. The supernatant was discarded. The worms were resuspended in 10 mL of 0.1 M NaCl and allowed to settle. Early larval stages were removed by aspiration. Adult worms were treated with a solution of 1.1% sodium hypochlorite (Clorox bleach) and 0.55 M NaOH to dissolve the cuticle of adults and released the eggs into the solution. The eggs were pelleted by centrifugation at 800 x g for 5 s, washed twice with 10 mL sterile water (800 x g, 30 s), transferred to M9 buffer (86 mM NaCl, 42 mM Na₂HPO₄, 1 mM MgSO₄) and allowed to hatch overnight at 20°C (75).

Preparation of hemin chloride

Aliquots of 10 mM hemin chloride was prepared by dissolving 130 mg hemin chloride in 18 mL of 0.3 M NH₄OH, and the pH was adjusted to 8.0 using concentrated HCl. The final volume was calibrated to 20 mL with 0.3 N NH₄OH, pH 8.0. The solution was sterilized using a 0.22 µm syringe top filter (Millipore, Billerica, MA) and stored at -20°C for up to one week. Zinc mesoporphyrin and gallium protoporphyrin IX were freshly prepared using the same method except these solutions were not filter sterilized. All porphyrin compounds were purchased from Frontier Scientific (Logan, UT).

Zinc mesoporphyrin assay

N2 and *them C. elegans* strains were synchronized, and approximately 500 L1 larval stage worms were transferred to 10 cm RNAi plates seeded with HT115(*DE3*) *E. coli*. These plates were incubated at 15°C for 72 h. Worms were washed from plates with M9 buffer into microcentrifuge tubes. To remove any residual bacteria, the tubes were placed on ice for 10 min, the supernatant was aspirated, and the worm pellet was washed twice with M9 buffer. The worms were transferred to 12-well plates containing mCeHR-2 media supplemented with 4 µM hemin and 10 µM ZnMP overnight at 20°C with shaking. Worms were subsequently moved to microcentrifuge tubes, pelleted by recentrifugation at 800 x g for 1 min, resuspended with M9 buffer, and allowed to settle by gravity on ice for 10 min. The supernatant was aspirated to remove any precipitated ZnMP in the liquid media. Worms were washed a second time with 500 µl of M9 buffer, incubated with shaking for 30 min to remove residual ZnMP from the lumen of their intestines, and immobilized with 10 µM levamisole. Worms were then transferred to a 2 % agar pad affixed to microscope slides. Differential interfering contrast (DIC) and fluorescent images were collected using a CCD camera attached to a Leica DMIRE2 epifluorescence/DIC microscope fitted with a Rhodamine filter.

Gallium Protoporphyrin IX toxicity assay

P₀ N2 and *them C. elegans* strains were grown in mCeHR-2 supplemented with 1.5µM heme and synchronized. Approximately 500 F₁ L1 stage worms were transferred to 10 cm RNAi plates seeded with HT115(*DE3*) containing pL4440 plasmid targeting a gene of interest for knockdown. Worms were incubated at 15°C for 72 h. Worms were washed

from the plates with M9 into microcentrifuge tubes. Approximately 50 L4 larval stage worms were transferred to 12-well RNAi plates supplemented with different concentrations of gallium protoporphyrin IX (GaPP). Worms were incubated at 20°C for 24 h. In each well, the number of live worms was counted and divided by the total number of worms originally transferred to determine the percentage of worms that survived. Each RNAi construct was analyzed in duplicate.

Cloning of RNAi constructs

Constructs which were unavailable in either the Ahringer or Vidal RNAi feeding library were cloned using the TA cloning method. pL4440 plasmid DNA was linearized with *EcoRV* and incubated with *Taq* polymerase with only dTTP at 72°C for 1 h. The linearized pL4440 was subsequently incubated with T4 DNA ligase (Fermentas, Ontario, Canada) overnight at 15°C to ligate plasmids which did not contain 'T' overhangs. The ligation reaction was resolved on a 0.8 % agarose gel to separate the ligated circular from the linearized plasmids. Linear pL4440 was purified using Nucleospin PCR purification kit (Macherey-Nagel, Düren, Germany). Primers were designed to amplify a 500-base pair exon fragment of the target gene by PCR using *Taq* polymerase. Linear pL4440 plasmid and purified PCR product were incubated with T4 DNA ligase at 15°C overnight. One µl of each ligation reaction was used to transform HT115(*DE3*) *E. coli* by electroporation. Clones were confirmed by colony PCR. Positive clones were purified extracted with Nucleospin Plasmid Miniprep (Macherey-Nagel, Düren, Germany) and were sequenced at the University of Maryland, College Park Genomics Core Facility.

Brood size assay on *hemB* bacteria

E. coli strain RP523 (*hemB*) was grown in LB broth supplemented with 2 μ M heme overnight at 37°C. This culture was then split at a ratio of 1:5 and 1:12 in fresh LB supplemented with 2 μ M and 50 μ M heme. The cells were grown aerobically at 37°C to an OD₆₀₀ of 1.0. The cultures were diluted to an OD₆₀₀ of 0.1 and used to seed 35 mm NGM plates. Synchronized N2 and *them* P₀ L1 larval stage worms were transferred to 2 μ M and 50 μ M *hemB* plates and incubated at 20°C for six days. Ten F₁ L4 larval stage worms were transferred to individual fresh plates seeded with *hemB* supplemented with 2 μ M and 50 μ M heme. Every two days, each of the F₁ worms were transferred to a new NGM plate seeded with *hemB* until the individual worms stopped laying eggs. The progeny from individual F₁ was counted from each plate and added together to determine the total brood size of each F₁ hermaphrodite.

Male Production

Males were created by three different methods-heat shock, ethanol treatment, and RNAi. For the heat shock method, P₀ L4 larval stage N2 and *them* hermaphrodites were transferred to 35 mm NGM plates. Plates were sealed with parafilm and incubated at 30°C for 4 h. The plates were then transferred to 20°C and incubated for 3 days. F₁ progeny was examined for males by microscopy. For the ethanol treatment method, 30 L4 larval stage N2 and *them* hermaphrodites were transferred to a microcentrifuge tube containing 10 % ethanol and incubated at room temperature for 30 min. Worms were subsequently washed with M9, transferred to 60 mm NGM plates seeded with OP50, and incubated at 20°C for 3 days. F₁ progeny was examined for males by microscopy (76).

For the RNAi method, 10 cm RNAi plates were seeded with HT115(*DE3*) bacteria induced to synthesize *him-14* (*high-incidence of males 14*) dsRNA. Five P₀ L4 larval stage N2 and *them* hermaphrodites were transferred to the 10 cm RNAi plates and incubated at 15°C for two generations. F₂ progeny was examined for males by microscopy (77). Males were maintained by setting up crosses with males and hermaphrodites to produce 50 % males in the following generation.

Mating efficiency assay

Males were generated using the *him-14* RNAi method. The HT115(*DE3*) bacteria was cultured in LB+carb+tet supplemented with either 0 μM or 200 μM heme. After two generations on the RNAi plates, male worms were identified and picked on to 30 mm plates seeded with OP50 which was cultured in LB supplemented with either 0 μM or 200 μM heme. F₂ *them* males were crossed with N2, *them*, and BA17 (*fem-1*) hermaphrodites with a ratio of five males to one hermaphrodite and allowed to mate for 48 h at 20°C. After 48 h the hermaphrodites were individually placed on 30 mm plates seeded with OP50 which was cultured in LB supplemented with either 0 μM or 200 μM heme. These plates were incubated at 20°C and after 3 days the number of males and total progeny were quantified using microscopy.

Pyrosequencing

A representative *them* strain from each of the five complementation groups was crossed with CB4856 Hawaiian strain males. Fifteen hermaphrodites and 30 CB4856 males were placed on a 30 mm NGM plate and incubated at 20°C for 24 h. All P₀ hermaphrodites

which contained a mucosal plug in their vulva were moved to individual 30 mm NGM plates and incubated at 20°C for 2 days. Thirty of the F₁ progeny was transferred to an unseeded new plate at the L4 stage. F₂ progeny was transferred to a 6-well plate containing mCeHR-2 liquid media supplemented with 800 µM heme and incubated at 20°C with shaking. After 7 days of growth, 70 F₂ gravid progeny were transferred from the liquid media to individual unseeded NGM plates. Each F₂ hermaphrodite was considered a recombinant line. After 24 h of laying eggs, the F₂ gravids were transferred to fresh NGM plates seeded with OP50. From the unseeded plate, 10 F₃ L1 larval stage worms from each plate were transferred to individual wells of a 96-well plate containing mCeHR-2 liquid media supplemented with 800 µM heme and incubated at 20°C. After 7 days, F₃ progeny was examined for growth. Lines which passed a stringency of 8 out of 10 F₃ progeny growing to gravid, were grown *en masse* and genomic DNA was extracted.

Identification of single nucleotide polymorphisms (SNPs) for analysis in *them* mutants was done using the database described in Wicks *et al.* (78). Primer sequences were either derived from Bruinsma *et al.* (65) or were generated using Biotage Primer Design software. Pyrosequencing was performed on the PyroMark Q96 ID System following the protocol provided by the manufacturer Biotage AB (Uppsala, Sweden). SNPs were analyzed by determining the presence of a N2 SNP or Hawaiian (HA) SNP. SNPS were assigned a possible score of 2. The presence of a homozygous N2 SNP was assigned a score of 2, a heterozygous N2 SNP was assigned a score of 1 and a homozygous HA SNP was assigned a score of 0. To determine the recombination frequency, scores from each recombinant line were added together and divided by the highest score possible.

Two-factor recombination mapping

C. elegans strains CB713 [*unc-67(e713)*] and CB524 [*unc-70(e524)*], were chosen for two-factor recombination mapping. CB713 or CB524 strain males were crossed with *them* hermaphrodites at 20°C. After 24 h, each of the P₀ hermaphrodites was transferred to an individual 30 mm NGM plate and incubated at 20°C for 3 days. F₁ L4 larval stage worms were transferred into individual wells of a 48-well plate containing mCeHR-2 media supplemented with 800 μM heme incubated at 20°C with shaking. Thirty F₁ L4 worms were only transferred from plates which contained males, which is indicative of a successful mating. After 7 days, the F₂ progeny were transferred to microscope slides and examined for growth by microscopy. Worms which grew to gravid were transferred from the slide to individual 35 mm NGM plates seeded with OP50 bacteria. The plates were maintained at 20°C, and the F₃ progeny was examined by microscopy for the presence of the uncoordinated movement phenotype. Any line which showed growth and uncoordinated movement were further screened to confirm presence of *them* allele. Five F₄ L4 larvae from each potential recombinant line were transferred to a 30 mm unseeded NGM plate and incubated at 20°C overnight. Ten F₅ L1 larval stage worms of each potential recombinant line were transferred to individual wells of a 96-well plate containing mCeHR-2 liquid media supplemented with 800 μM heme. If they passed a stringency of 8 out of 10 growing to gravid, the line was counted as a true recombinant. Recombination frequency was determined by dividing the number of recombinants by the total number of worms screened.

Deficiency mapping

Thirty IQ9110 males were crossed to 15 BC1283 (*eT1/sDf20*) hermaphrodites on a 30 mm NGM plate at 20°C overnight. The P₀ hermaphrodites were transferred to individual unseeded NGM plates incubated at 20°C overnight. From the unseeded plates, 100 F₁ L1 larval stage worms were placed in individual wells of two 96-well plates containing mCeHR-2 media supplemented with 800 μM heme. These two plates were incubated at 20°C for 7 days. F₁ progeny which grew was counted and divided by the total number of progeny screened to determine whether the IQ9110 mutation was present in the *sDf20* deletion region.

Sanger DNA sequencing

Sequencing was performed using BigDye Terminator (Applied Biosystems, Foster City, CA). The sequencing was performed using capillary electrophoresis with either a 3100 or a 3730 sequencing instrument (Applied Biosystems Foster City, CA) at the University of Maryland, College Park Genomics Core Facility. Sequencing files were analyzed using Vector NTI software (Invitrogen, Carlsbad, CA).

Genome sequencing

Genomic DNA of IQ7280, IQ7310, IQ8280, and IQ9110 was extracted using DNeasy Blood & Tissue Kit (Qiagen, Valencia, CA). Sequencing was performed with an Illumina Genome Analyzer machine (Illumina, San Diego, CA). Genomic sequence data was analyzed by Dr. Harold Smith (NIDDK, NIH) using Mapping and Assembly with

Qualities software to align the fragments created from genomic sequencing. All genome sequencing was carried out at the NIH, Bethesda, Maryland campus.

Microinjection of rescue construct

Approximately 100 synchronized IQ9110 L1 larval stage worms were transferred to NGM plates seeded with OP50 and incubated at 20°C for 3 days. Worms were considered ready for injection once they contained a full row of embryos within the uterus. Worms to be injected were removed from the NGM plate and placed on a 2 % agarose pad coated with a thin layer of immersion oil. The rescue construct, which consists of the promoter, gene, and 3'UTR, was amplified with iProof (BioRad, Hercules, CA) and purified by Nucleospin PCR Purification Kit (Macherey-Nagel, Düren, Germany). The rescue construct (50 ng/μl) was mixed with a dominant marker (50 ng/μl), *rol-6*, at a 1:1 ratio and were coinjected into IQ9110 worms (79). Rescue lines carrying the *rol-6* marker can be easily identified by the Rolling phenotype. The final concentration of the rescue construct and *rol-6* plasmid was 50 ng / μl. The DNA mixture was loaded into a microinjection needle and manipulated with a Narashige hanging joystick micromanipulator. The DNA was injected into the gonads of young gravid P₀ worms with a Femtojet (Eppendorf, Hauppauge, New York) set at 20.5 psi. After injection, worms were allowed to recover by placing them on NGM agar plates seeded with OP50 and incubated at 20°C for 3 days. F₁ progeny with the rolling phenotype were transferred to individual NGM OP50 plates. After three days, plates were checked for F₂ progeny with the rolling phenotype. F₂ rollers are an indication that the rescue construct was segregating. These worms were maintained as

extrachromosomal lines. Each F₂ roller was further propagated as a separate rescue line for experiments. The 8 rescue lines were created and labeled separately from 1-8 (IQ9110/*nhr-14*).

Toxic heme resistance rescue experiment

Approximately 30 P₀ N2 wild-type, IQ9110, IQ9110/*nhr-147-7*, and VC1585 (*nhr-147*) L4 larval stage worms were transferred from NGM OP50 plates into the individual wells of two 96-well plate. Each well of the 96-well plates contained 100 µl of mCeHR-2 media supplemented with 800 µM heme and were incubated at 20°C with shaking for 7 days. After 7 days, the F₁ population was extracted from each well and transferred to an unseeded NGM plate. F₁ worms were analyzed by microscopy and worms which showed growth were divided by the total worms to obtain the percent growth.

Chapter 3: Results

A forward genetic screen to identify toxic heme resistant mutants

A common method used in *C. elegans* for identifying novel genes involved in a variety of biological processes is a random mutagenesis screen, which causes point mutations throughout the worms' genome, potentially disrupting a gene involved in the biological process being studied. To identify novel genes involved in heme homeostasis, Dr. Anita Rao performed a EMS mutagenesis screen in *C. elegans* to identify mutants which were resistant to toxic levels of heme (Rao and Hamza, personal communication). Wild-type N2 Bristol strain worms were mutated with methylsulfonic acid, ethyl ester in mCeHR-2 medium to identify surviving worms which could grow and reproduce at 800 μ M heme, a concentration which causes growth arrest in wild-type worms (14). A total of 300,000 haploid genomes were screened for growth, and 13 independent strains were identified (Appendix A). These mutants were termed *them* for Toxic HEMe resistant mutants and all of the mutations were found to be recessive. Additionally, each of these lines was further characterized by examining their growth in mCeHR-2 supplemented with the following concentrations of heme: 1.5 μ M, 20 μ M, 800 μ M and 1 mM. Based on their growth phenotype, they were organized into three different phenotypic clusters (Appendix B). Class A showed enhanced growth when compared to N2 at 1.5 μ M and exhibited resistance at 1 mM heme. Class B contained a single mutant, IQ8280, which also showed enhanced growth when compared to N2, exhibited resistance at 800 μ M heme, but showed growth arrest at 1 mM. Class C grew similar to N2 at 1.5 μ M and depending on the strain, exhibited resistance at 800 μ M or at 1 mM heme.

To determine if any of these lines contained mutations within the same gene, complementation mapping was performed by Brian Le, an undergraduate student. Each of these 13 strains was placed into five complementation groups (Appendix C). The following sample strains were chosen from each of these complementation groups for mapping and further characterization: strain IQ7280 from group one, strain IQ7310 from group two, strain IQ8280 from group three, strain IQ1068 from group four, and strain IQ9110 from group five.

Genetic mapping by pyrosequencing identifies the genomic locus for *them* mutations

To map the genetic lesion responsible for *them* phenotype, each of the sample *them* strains from the complementation groups were crossed to the Hawaiian mapping strain CB4856 (HA) (65). CB4856 is a *C. elegans* strain that was discovered in Hawaii, and naturally contains single nucleotide polymorphisms (SNPs) which differ from the commonly used laboratory strain N2, isolated in Bristol, England. Since *them* mutants were generated in the N2 wild type strain, SNPs in proximity to the mutations will be linked to the N2 strain and not HA.

To identify the genetic region around the mutation, *them* and CB4856 strains were crossed to obtain F₁ progeny which were allowed to self fertilize. Consequently, the F₂ recombinants, will contain a heterogeneous mixture of N2 and HA SNPs randomly dispersed throughout their genomes. During meiosis of the heterozygous progeny, *them* mutations and thus the N2 SNPs in close proximity would not sort independently as a result of genetic linkage. Thus, recombinant lines that are resistant to 800 μM heme will

contain the greatest percentage of SNPs concentrated close to the genomic locus containing *them* lesions.

To quantify the percentage recombination between the N2 and HA SNPs present in the recombinant lines, we used pyrosequencing. The PyroMark Q96 ID instrument tracks each nucleotide added to the reaction, and quantifies the number of nucleotides being added to the complementary single stranded DNA. This is performed by sensing the amount of light produced by the firefly enzyme luciferase which catalyzes a reaction every time a nucleotide is added (18). Through this method, a stoichiometric ratio of N2 versus HA SNPs located throughout a chromosome can be generated.

To produce *them* recombinant lines, Dr. Anita Rao crossed CB4856 males with *them* to create heterozygous F₁ progeny. The F₁ progeny self-fertilized and the resulting F₂ progeny was screened for toxic heme resistance. F₂ worms that showed heme resistance were not considered true recombinant lines until their F₃ progeny were screened for growth a second time in mCeHR-2 media supplemented with 800 μM heme. Lines that passed the second round of screening provided a more precise recombinant map and contained a higher percentage of N2 SNPs around the genetic region in which the *them* mutations were located. Each recombinant line was grown on a 10 cm NGM plate seeded with OP50 to extract their genomic DNA. IQ7280 provided 31 recombinant lines, IQ7310 provided 28 recombinant lines, IQ8280 provided 23 recombinant lines, and IQ9110 provided 18 recombinant lines. Recombinant DNA samples were collected for IQ1068; however, no clear segregation could be confirmed and therefore, mapping of this strain was terminated.

To first determine the chromosomal location of *them* mutations, we examined individual SNP markers located in approximately the center of each of the six chromosomes. This was performed by determining the percentage of N2 SNPs at a particular SNP marker. To quantify the percentage of N2 SNPs, for each recombinant line the number of N2 SNPs present was added together with the total SNPs (N2 + HA) in all recombinant lines. The SNPs analyzed were *pkP1057* (Chr I), *pkP2148* (Chr II), *pkP3051* (Chr III), *pk4064* (Chr IV), *pkP5513* (Chr V) and *amP117* (Chr X) (65). The results from the pyrosequencing showed IQ7280, IQ7310 and IQ8280 mapped to chromosome I, while IQ9110 mapped to chromosome V (Table 1).

SNPs at the distal ends and directly to the left and right of the center SNP on chromosome I and V were further examined to identify the approximate region *them* mutations mapped. SNPs localized to these regions were examined to more accurately determine the genetic interval in which *them* mutations were located. Primers were designed to amplify approximately a 200 base-pair fragment which contained the SNP. The Biotage Primer Design software designed three primers, two of which PCR amplified the fragment and a third which annealed a few base pairs away from the SNP to be interrogated (Appendix D). All primers were designed to avoid secondary structures and for optimal annealing temperature. Once seven different SNPs had been analyzed along chromosomes I and V for each of the recombinant lines, a recombinant map was created for each line. This recombinant map was examined for irrelevant recombination patterns, such as alternating N2 and HA SNPs or evidence of more than one recombination event occurring. Recombinant lines which shared these characteristic were removed from the sample pool to provide a more accurate recombination map of

them strains. From IQ7280 six lines were removed, from IQ7310 four lines were removed, from IQ8280 four lines were removed, and from IQ9110 four lines were removed. New SNP markers were analyzed until the genetic region which mapped 100% N2 SNPs had no useful SNPs for further analysis. The location of *them* mutation was found to be between SNPs *ihP1* (-5.3 centimorgan (cM)) and *amP108* (-5.2 cM) for strain IQ7280, and between SNPs *ihP1* (-5.3 cM) and *ihP2*(-4.5 cM) for strain IQ7310 and between *ihP1*(-5.3 cM) and *ihP3* (-3.8 cM) for strain IQ8280 on chromosome I. Strain IQ9110 was found to map to a single SNP *pkP5513* (+0.1 cM) on chromosome V (Fig. 1 & Table 2).

Two-factor and deficiency mapping confirms pyrosequencing

To confirm the SNP mapping by pyrosequencing, we utilized two-factor recombination mapping. This technique estimates the genetic distance between two mutant alleles by assessing the recombination frequency. Three-factor mapping using strains MT464 and MT465 had been attempted previously with little success. The difficulties lay with moving from NGM agar plates, on which genetic crosses were performed, to mCeHR-2 liquid medium, which was used to assess the heme resistant phenotype. Furthermore, the phenotypes of the mapping strains interfered with the heme resistant phenotype by preventing growth, and therefore, prevented scoring for the recombination frequency. To avoid these issues we conducted two-factor recombination mapping.

The strain CB713 carries a mutation in the gene *unc-67* which produces an uncoordinated movement phenotype. This gene is located at -2.51 on chromosome I and

was chosen for its proximity to the mapped genetic region for IQ7280, IQ7310 and IQ8280. Strain CB524 has a mutation in *unc-70* which also produces an uncoordinated movement phenotype. This gene is located at +0.5 cM on chromosome V and was chosen for its proximity to the mapped location for IQ9110.

CB713 homozygous males were crossed with IQ7280, IQ7310, IQ8280 hermaphrodites. F₁ progeny, heterozygous for *them* and *unc*, were transferred to mCeHR-2 media supplemented with 800 μM heme and allowed to produce F₂ progeny. All F₂ progeny were counted and classified as either adults or growth arrested. Worms that grew to the adult stage were placed on individual plates to follow their F₃ progeny for the presence of the *unc* phenotype. Lines with both *them* and *unc* phenotypes were screened a second time for resistance to toxic concentrations of heme before they were counted as a full recombinant line.

To determine the genetic distance between *them* and *unc* mutations, the number of recombinant lines was divided by the total number of F₂ progeny screened. IQ7280 was calculated to have a distance of 0 cM, IQ7310 was calculated to have a distance of 1.56 cM, and IQ8280 was calculated to have a distance of 0.7 cM between *them* and *unc-67*. IQ9110 was calculated to have a distance of 0.25 cM between *them* and *unc-70*. Results from two factor recombination mapping indicated that the *unc-67* and *unc-70* alleles were in close proximity to *them* mutations that were identified by SNP mapping (Table 3).

Another approach to determine the location of each *them* mutation was deficiency mapping. Strain BC1283 carries a deletion in chromosome V between -0.9 cM and +0.6 cM. This deletion is balanced by a region from chromosome I which allows the worm to remain viable and produce progeny. BC1283 hermaphrodites were crossed with IQ9110

males. The F₁ progeny were placed in mCeHR-2 media supplemented with 800 μM heme to screen for resistance. If the mutation is located within the region of the deletion, then fifty percent of the progeny would grow to gravid. If the mutation was located outside the region of the deletion then all of the progeny would be growth arrested. Forty-four percent of the heterozygous BC1283/IQ9110 F₁ progeny grew to the gravid stage. This indicated the presence of IQ9110 *them* mutation within the region of -0.9 cM to +0.6 cM (Table 3).

In summary, multiple SNPs and mutant strains were used to map *them* mutations. To determine the approximate location of IQ7310, IQ7280, and IQ8280 mutations, twelve SNPs were analyzed by pyrosequencing and one mutant strain was used for two-factor recombination mapping. To identify the approximate location for IQ9110, nine SNPs were analyzed by pyrosequencing, one mutant strain was used for two-factor recombination mapping, and a deletion strain was used for deficiency mapping (Fig. 1). These corroborative results permitted us to create a genetic map with the location of *them* mutation with high confidence.

Gallium protoporphyrin IX RNA interference screen identifies candidate genes within the mapped genetic interval

Once the genetic interval in which *them* mutations had been narrowed down, the genes within this region had to be systematically analyzed to determine if they are responsible for the *them* phenotype. IQ7280, IQ7310, and IQ8280 mapped to a region between -8.0 cM and -3.2 cM on chromosome I which contained 114 genes (Table 4).

To identify the *them* mutation, we needed to phenocopy or recapitulate the *them* phenotype by RNAi of candidate genes within this genetic interval.

The toxic heme resistant phenotype is only visible in mCeHR-2 axenic liquid medium because of the high solubility of hemin chloride in this growth medium. However, due to insolubility issues with heme, worms do not exhibit this phenotype on NGM agar plates. Moreover, the RNAi feeding bacterial strain HT115(*DE3*) cannot be grown in the nutrient rich mCeHR-2 medium because it causes rapid bacterial growth and quickly outgrows the worms being cultured. Since approximately 114 genes needed to be screened within the genetic interval, microinjecting dsRNA targeting each gene would be a tedious and time-consuming process. We therefore sought *them* phenotypes that were easily identifiable and quantifiable on NGM agar plates.

The heme analog, gallium protoporphyrin IX (GaPP), is 800 fold more toxic than heme (14). Gallium replaces the iron atom located in the center of the protoporphyrin ring, but unlike iron, gallium is not redox-active and if any hemoprotein incorporates GaPP, it becomes non-functional. Previous work by Dr. Anita Rao showed that IQ7280, IQ7310 and IQ8280 were resistant to GaPP in mCeHR-2 liquid medium, but not IQ9110 (Appendix E). To recapitulated the GaPP resistance phenotype in liquid to NGM agar plates, we used synchronized worms (P_0) from mCeHR-2 media supplemented with 1.5 μM heme to increase the sensitivity of F_1 progeny to the heme analog GaPP. F_1 worms at the L1 larval stage were transferred to two different RNAi plates seeded with *E. coli* HT115(*DE3*) induced to synthesize dsRNA. After 72 hours of growth at 15°C, approximately 50 L4 larvae were transferred to 12-well plates containing GaPP in NGM agar and HT115(*DE3*). These worms were examined for resistance after growing for 24

hours on GaPP. When compared to N2 wild-type worms treated with vector only, all three *them* strains exhibited resistance at 4 μ M GaPP in the F₁ generation (Figure 2). This provided an easily discernable phenotype on plates which could be used to screen candidate genes which phenocopies *them* mutant phenotype.

The Ahringer and Vidal RNAi libraries, which together cover 92% of the *C. elegans* genome, provided constructs targeting 103 of the 114 genes which needed to be analyzed. These clones were first sequenced to determine if they would be disrupting the targeted gene. Of these clones, 86 were found to be correct, we therefore cloned the remaining 28 constructs (Appendix F). The 114 genes were screened in the presence of 0 μ M, 2 μ M, and 4 μ M GaPP (Table 4).

From the initial screen, 30 candidate genes were identified that exhibited GaPP resistance when depleted. Rescreening the 30 genes resulted in the identification of only 19 genes which exhibited resistance to GaPP (Figure 3). These candidate genes coded for proteins with putative functions that included chromatid cohesion, metalloproteases, ribosomal proteins, RNA polymerases, and ubiquitin ligases (Table 5). Because of the unusual number of false positives, we decided to use another assay, described in the following section.

Further characterization of *them* phenotypes

The fluorescent heme analog zinc mesoporphyrin (ZnMP) was utilized to analyze intestinal heme uptake of *them* mutants. The structure of ZnMP differs from that of heme in that the vinyl side chains of heme are replaced by ethyl side chains and the iron atom is replaced by zinc. Since ZnMP is similar in structure to heme, it is proposed that ZnMP

transport utilizes heme transport pathways in the worm intestine (14). This assay provides a quantitative and qualitative measure of accumulation of fluorescent ZnMP.

N2 and *them* worms at the L4 larval stage were exposed to mCeHR-2 media supplemented with 10 μ M ZnMP overnight. Images of these worms were taken using a Leica inverted microscope equipped with a rhodamine filter (Fig. 4a). When images of N2 wild-type were compared with IQ7280, IQ7310, and IQ8280, each appeared to have reduced ZnMP uptake (Fig 4b). However, IQ9110 exhibited wild-type uptake of ZnMP.

To further characterize *them* mutants, brood size was examined in *them* and wild type strains. Since bacteria synthesize heme which is available for consumption by *C. elegans*, we were unable to use the commonly used *E. coli* strains – OP50 and HT115(*DE3*) - for *C. elegans* growth. Instead, we used *E. coli* strain *hemB* which lacks ALAD, the second enzyme in the heme biosynthesis pathway. Growth of *hemB* bacteria is directly dependent upon heme supplemented in the growth medium. *hemB* was grown in LB supplemented with either low (2 μ M) or high (50 μ M) heme to OD₆₀₀ 1.0, and NGM plates were seeded with equal numbers of bacteria. The following day, a synchronized population of P₀ N2 and *them* L1 worms were added to *hemB* plates and grown till the L4 larval stage. The P₀ L4 worms were then transferred to new *hemB* agar plates. After the F₁ progeny had been laid, ten L4 hermaphrodites from the F₁ generation of each strain were placed on individual *hemB* plates and transferred every two days until they stopped laying eggs. The plates with eggs were given 24 hours to hatch, and the live progeny was counted. We found that at high heme, IQ7310 and IQ7280 had a brood size similar to N2 (Fig. 5A). However, IQ9110 had a significant reduction in brood size-a phenotype that was exacerbated in IQ8280. At low heme, the IQ8280 brood size was

significantly larger than the N2 wild-type (Fig. 5B). IQ7310 showed a reduction in brood size while no change was observed for IQ7280. Interestingly, heme did not increase the number of progeny from IQ9110.

A male mating defect phenotype was identified during attempts to produce males for two factor recombination mapping. Three of the mutant strains-IQ7280, IQ7310 and IQ8280-were unable to produce males that mated efficiently. The standard method of crossing a wild-type N2 male with *them* hermaphrodites failed to produce male progeny with heme resistance at the expected segregation of 25% progeny. Attempts to make homozygous males using ethanol treatment and heat treatment also failed to produce males since both of these methods adversely affected *them* hermaphrodites. Knocking-down the high incidence of male 14 (*him-14*) gene using RNAi by feeding HT115(*DE3*) was successful in producing homozygous males. The male mating defect was first identified when attempts to mate *them* males with *them* hermaphrodites failed to produce males in the subsequent generation.

To determine if IQ7280, IQ7310, and IQ8280 male sperm was the cause of the mating defect, *them* males were crossed to a feminized *C. elegans* strain. BA17 worms have a mutation in *fem-1* which causes feminization of the germline, thereby converting a hermaphrodite into a female worm. If a successful mating did not occur, the BA17 female will not produce any progeny at 20°C. After crossing IQ7280, IQ7310, and IQ8280 males to the BA17 strain, no progeny was observed (Fig. 6A). This indicated that either no mating took place, or *them* sperm was unable to fertilize the BA17 oocytes. This was not a general defect in *them* mutants, because IQ9110 mated successfully with

BA17 hermaphrodites (Fig. 6B). The presence or absence of heme did not alter the results of this experiment (Fig. 6A & 6B).

Additionally, *them* males were placed on a plate with *them* hermaphrodites to assess their mating behavior. Fifteen males were placed on a 35 mm NGM agar plate with 3 hermaphrodites and were observed under a dissecting scope for 30 minutes. N2 males carried out normal mating behaviors including seeking out the hermaphrodite, running the rays along the hermaphrodites cuticle and inserting spicules within the vulva for ejaculation. *them* males lacked all of these mating behaviors.

Whole genome sequencing to identify *them* mutations

As an alternative to sequencing the candidate genes from the GaPP RNAi screen, we used next generation sequencing technology to pinpoint the genetic lesion in *them* mutants. The four *them* strains which had been mapped with pyrosequencing were grown in axenic mCeHR-2 media supplemented with 800 μ M heme and the genomic DNA extracted for sequencing using the Illumina/Solexa platform. Dr. Harold Smith from the NIH, NIDDK used Mapping and Assembly with Qualities software to align the fragments created from genomic sequencing. The aligned genomes were then compared with the reference wild-type N2 genome to locate the possible mismatch by aligning nucleotides within the genomic locus narrowed by pyrosequencing. Only mismatches within the ORF were initially considered. The list of SNPs were narrowed down by only considering SNPs within the open reading frame (ORF) of genes. No SNPs were identified in ORFs within the expected genetic interval for IQ8280. Therefore, mutations

in 5' and 3' untranslated region were also examined. The genome sequencing provided a list of possible candidate genes which could now be examined for a possible role in heme homeostasis (Table 6).

Before each of these candidate genes could be examined for their role in the *them* phenotype, the mutations identified from genome sequencing were confirmed by directed sequencing. For each of the candidate genes, primers were designed to amplify the introns and exons. For the mutant IQ8280, primers were designed outside the 5' UTR. To provide high resolution sequencing, primers were designed at every 500 base pair interval (Appendix G). Of the 12 candidate mutations, nine were confirmed by directed sequencing. Background mutations present in all four *them* strains were re-sequenced in wild-type N2 to confirm their presence.

IQ7280 had three candidate genes confirmed by directed sequencing. One mutation caused a glycine to glutamic acid change in *lin-17*, a gene involved in the Wnt signaling pathway. Another mutation caused a glycine to glutamic acid change in Y47G6A.13, a putative casein kinase. The last mutation was in F40E3.2, a gene with an unknown function, converted a methionine into an isoleucine. This mutation, however, was also present in IQ7310. IQ7310 also had one other possible candidate gene with an unknown function, W03D8.5. This mutation converted a glutamic acid to lysine. A mutation within a putative 5' UTR of W03D8.5 was discovered during genome sequencing in *them* strain IQ8280. However, this mutation was not identified when directed sequencing was performed.

IQ9110 had three possible candidate genes that were confirmed by directed sequencing. K09H11.11, a gene with unknown function, contained a mutation that

converted a lysine to a glutamine. Another mutation converted a phenylalanine to leucine within *ttn-1*, a titan ortholog involved in muscle formation. The last mutation converted a glycine to cysteine in *nhr-147*, a nuclear hormone receptor.

Two mutations identified in all four *them* strains were theorized to be background mutations from our laboratory wild-type N2 strain. The first mutation was a methionine to isoleucine conversion in Y39G10AR.17, and the second was a histidine to tyrosine conversion in *ftn-1*. These mutations were sequenced in our wild-type N2 strain, and both were confirmed. Therefore, we no longer considered these mutations responsible for the toxic heme resistant phenotype in any of *them* strains.

To identify the mutant gene, RNAi was used to phenocopy a *them* phenotype. Although IQ9110 does not show any phenotype on plates, strains IQ7280 and IQ7310 showed four different phenotypes on plates: GaPP resistance, reduced ZnMP uptake, a male mating defect and heme-dependent brood size. Two of the possible *them* phenotypes on plates, GaPP resistance and reduced ZnMP uptake, could be phenocopied with RNAi. Therefore, the genes we analyzed further by RNAi were W03D8.5, F40E3.2, *lin-17* and Y47G6A.13 as these were possible candidate genes responsible for the *them* phenotype.

Through the GaPP RNAi screen, each of these genes had already been knocked-down to determine whether they exhibited GaPP resistance. After reexamining the results from this screen, no GaPP resistance was identified from any of these candidate genes (Fig. 3 & Table 5).

To examine whether depleting these candidate genes altered the uptake of heme, we used the ZnMP fluorescence assay. The controls for this experiment were N2,

IQ7280, IQ7310 and RNAi of *hrg-4*, a gene which encodes for a known intestinal heme transporter that has been shown to reduce uptake of ZnMP (36). Worms were exposed to 10 μ M ZnMP overnight, and microscopy images of these worms were acquired using a rhodamine filter (Fig. 7a). Depletion of W03D8.5 showed reduced ZnMP uptake, showed reduced ZnMP uptake, a phenotype that was comparable to that observed with IQ7310 (Fig 7b). This result indicated the possibility that a mutation in W03D8.5 may be responsible for the toxic heme resistant phenotype.

Another candidate gene identified by genome sequencing was *nhr-147*, a nuclear hormone receptor, in IQ9110. Nuclear hormone receptors are a class of transcription factors known to interact with heme. An example is REV-ERB α which is involved in circadian clock control (34). We therefore decided to rescue the IQ9110 mutant strain using wild-type *nhr-147*. The rescue construct consisted of a PCR product comprising the 3 kb region upstream of *nhr-147* translational start site, the *nhr-147* coding region (exons and introns), and 300 base pair region directly downstream of the translational stop site. The PCR product was sequenced, to ensure that there were no errors during DNA synthesis, and subsequently co-injected along with *rol-6*, a dominant marker, into IQ9110. We obtained eight rescue lines and chose line 7 because it showed the highest segregation of *rol-6* (26 %).

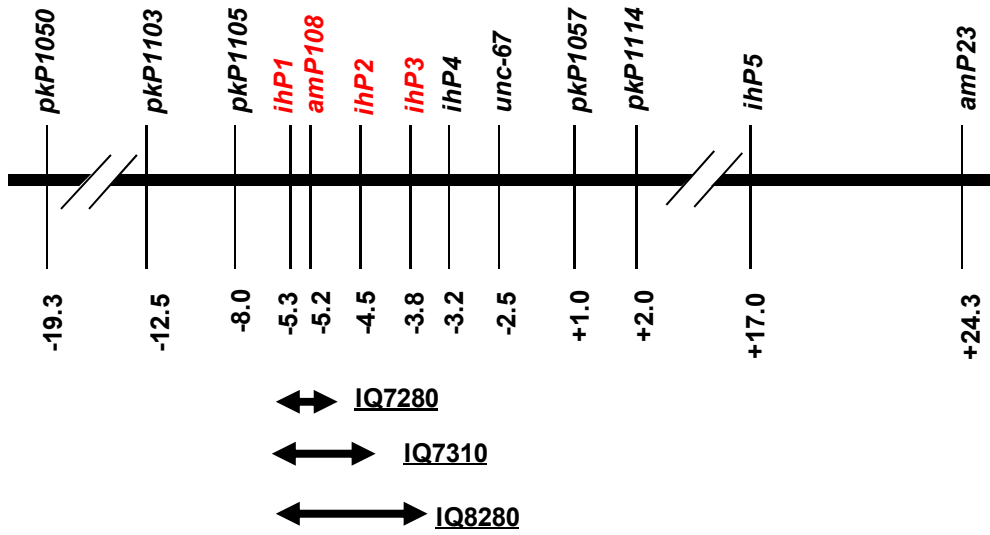
To determine if *nhr-147* was responsible for the *them* phenotype in IQ9110, a rescue experiment was designed to test its role in heme homeostasis. Because the initial selection of *them* mutants were based on their resistance to high heme (>800 μ M), we exposed wild-type N2, IQ9110, IQ9110 (*nhr-147*) and VC1585, which contains a deletion in *nhr-147*, to 800 μ M heme in mCeHR-2 and analyzed their progeny for loss in

resistance to heme toxicity (Fig. 8). Wild-type and VC1585 worms were growth arrested at the L3 larval stage. IQ9110 displayed 61 % of the total population exhibiting growth, and the IQ9110/*nhr-147* line 7 exhibited 35 % growth. A statistically significant difference in percentage growth between IQ9110 and IQ9110/*nhr-147* was observed. Additionally, the difference in percentage between IQ9110 and the IQ9110/*nhr-147* surpasses the percentage segregation of the rescue marker. Therefore, all of the worms which contain the rescue marker appear to be growth arrested. This result indicates that wild-type *nhr-147* rescues IQ9110 *them* phenotype and that the glycine to cysteine mutation in *nhr-147* may be responsible for the heme resistant phenotype.

Figure 1. A visualization of SNPs and mutant alleles used in mapping for chromosome I and V.

Each of the SNPs that were used for pyrosequencing and mutant alleles that were used for mapping are displayed at their approximate position in centimorgans on their respective chromosomes. Chromosome I contained 12 SNPs and one mutant allele which was analyzed. Chromosome V contained nine SNPs and one mutant allele which was analyzed. IQ7280, IQ7310, and IQ8280 all mapped to a similar region, represented by arrows on chromosome I. IQ9110 mapped to a single SNP on chromosome V. The SNPs that each of the *them* mapped to are labeled red.

Chromosome I



Chromosome V

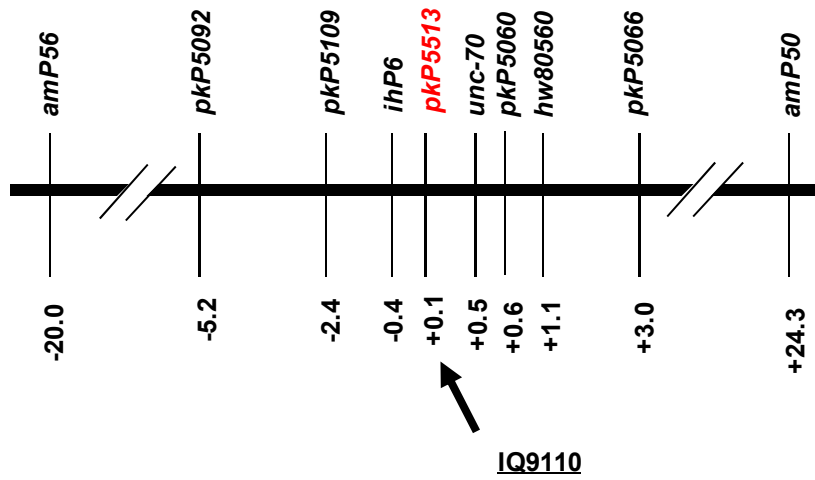


Figure 2. *them* mutants exhibit GaPP resistance

L1 larval stage worms of representative *them* strains were fed HT115(*DE3*) bacteria transformed with the empty vector for 72 hours. L1 larval stage N2 wild-type worms were fed HT115(*DE3*) bacteria producing dsRNA targeting *mrp-5* for 72 hours.

Approximately 50 L4 larval stage worms were transferred to 12-well RNAi plates seeded with HT115(*DE3*) producing dsRNA targeting vector or *mrp-5*. For each RNAi construct the following GaPP concentrations were tested: 0 μM , 1 μM , 1.5 μM , 2 μM , 3 μM , or 4 μM . They were exposed to GaPP for 24 hours. In each well, the number of live worms was counted and divided by the total number of worms originally transferred to determine the percentage of worms that survived. The experiments were performed in duplicate, and the data is presented as mean \pm SEM. A * indicates $P < 0.05$ and ** indicates $P < 0.01$ to display a significant difference between the strains and vector control at that specific GaPP concentration.

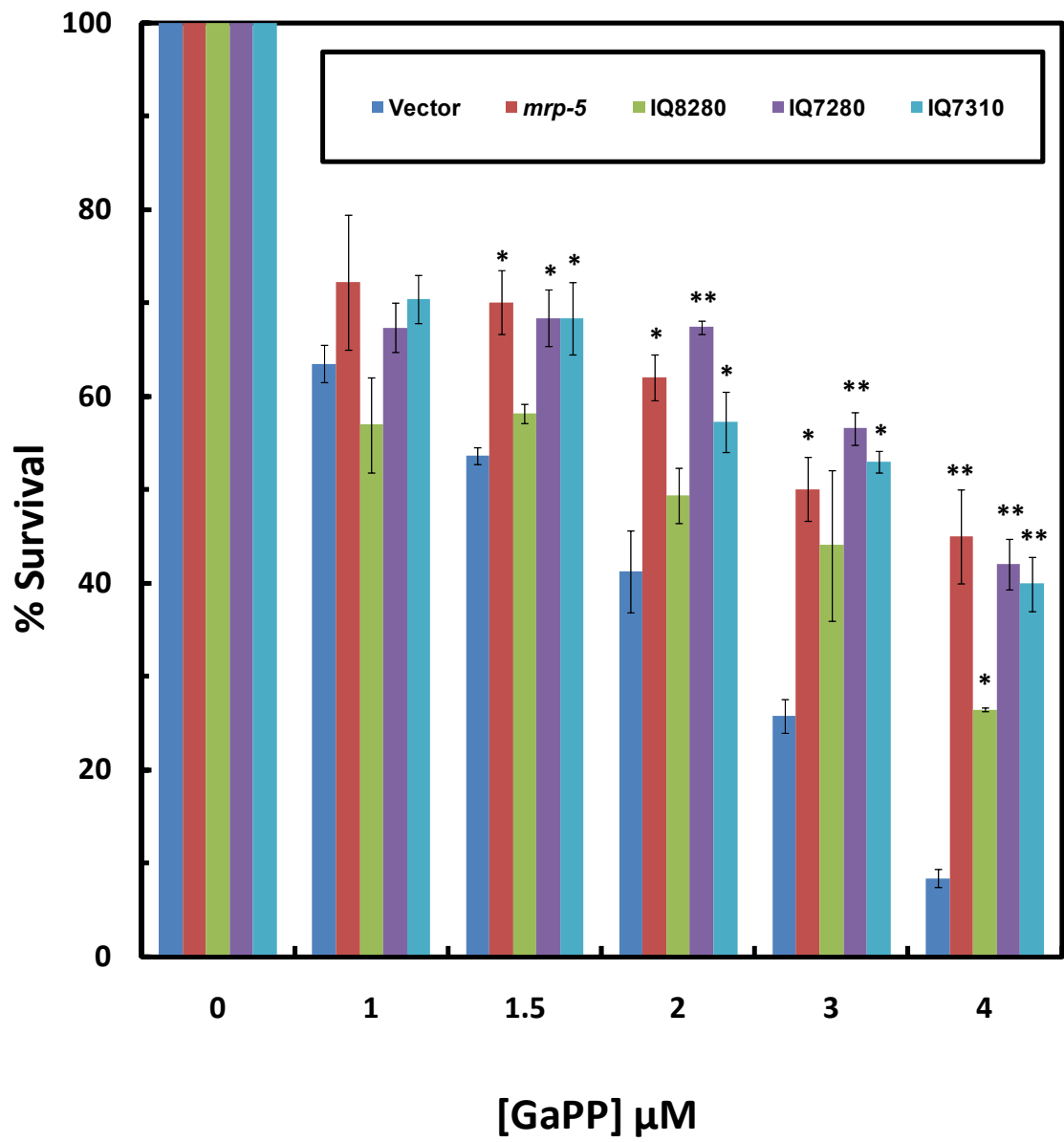


Figure 3. GaPP resistance screened in candidate genes for *them*

The candidate genes that were identified in the original GaPP screen were examined for resistance a second time. Synchronized L1 larval stage worms were treated with RNAi by feeding for 72 hours. Approximately 50 L4 larval stage these worms were transferred to a 12-well RNAi plate containing 0 μ M, 2 μ M, and 4 μ M GaPP. They were exposed to GaPP for 24 hours. In each well, the number of live worms was counted and divided by the total number of worms originally transferred to determine the percentage of worms that survived. The experiments were performed in duplicate, and the data is presented as mean \pm SEM.

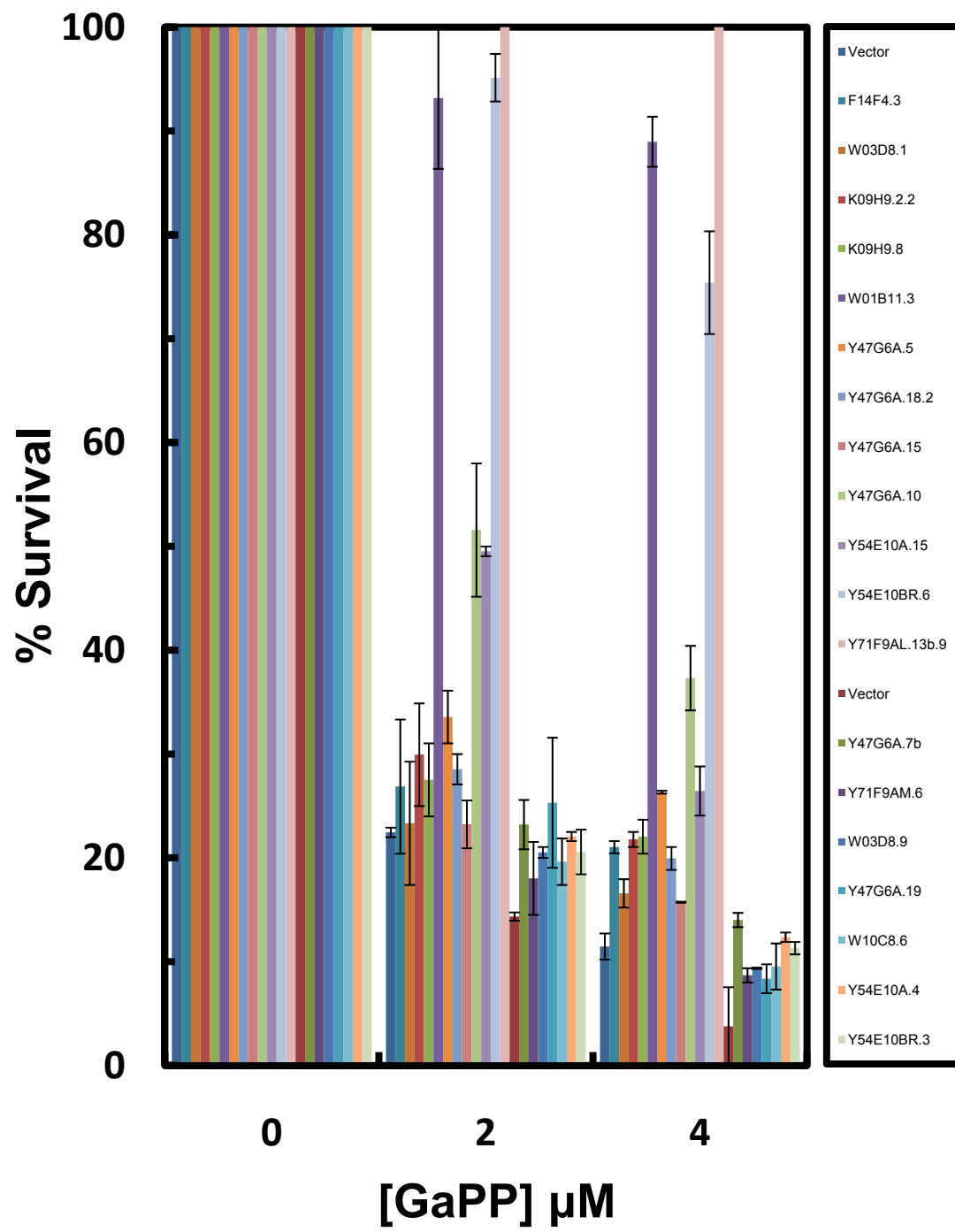
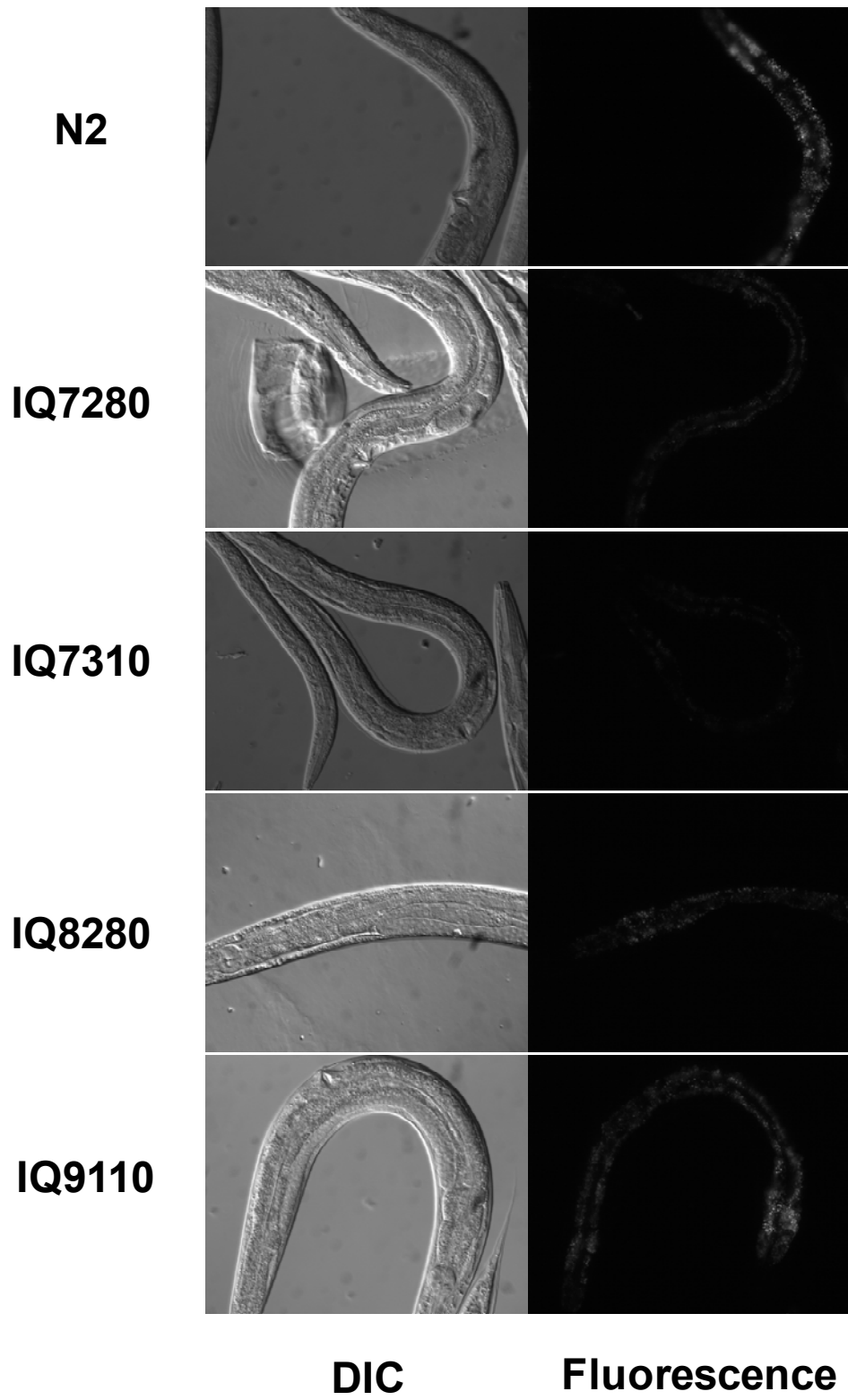


Figure 4. ZnMP uptake is reduced in *them*

L4 larval stage worms of the strains indicated were grown in mCeHR-2 media supplemented with 10 μ M ZnMP and 4 μ M heme at 20°C overnight. A) Images were taken using a CCD camera attached to a Leica DMIRE2 epifluorescence/DIC microscope fitted with a Rhodamine filter. The experiment was performed in duplicate. Images are representative of the overall uptake of each strain, n=4. B) The fluorescence was quantified using Simple PCI software and the data is reported as the mean \pm SEM. The * indicates P<0.05 and ** indicates P<0.01 to display a significant difference between *them* strains average fluorescence and N2 wild-type.

A



B

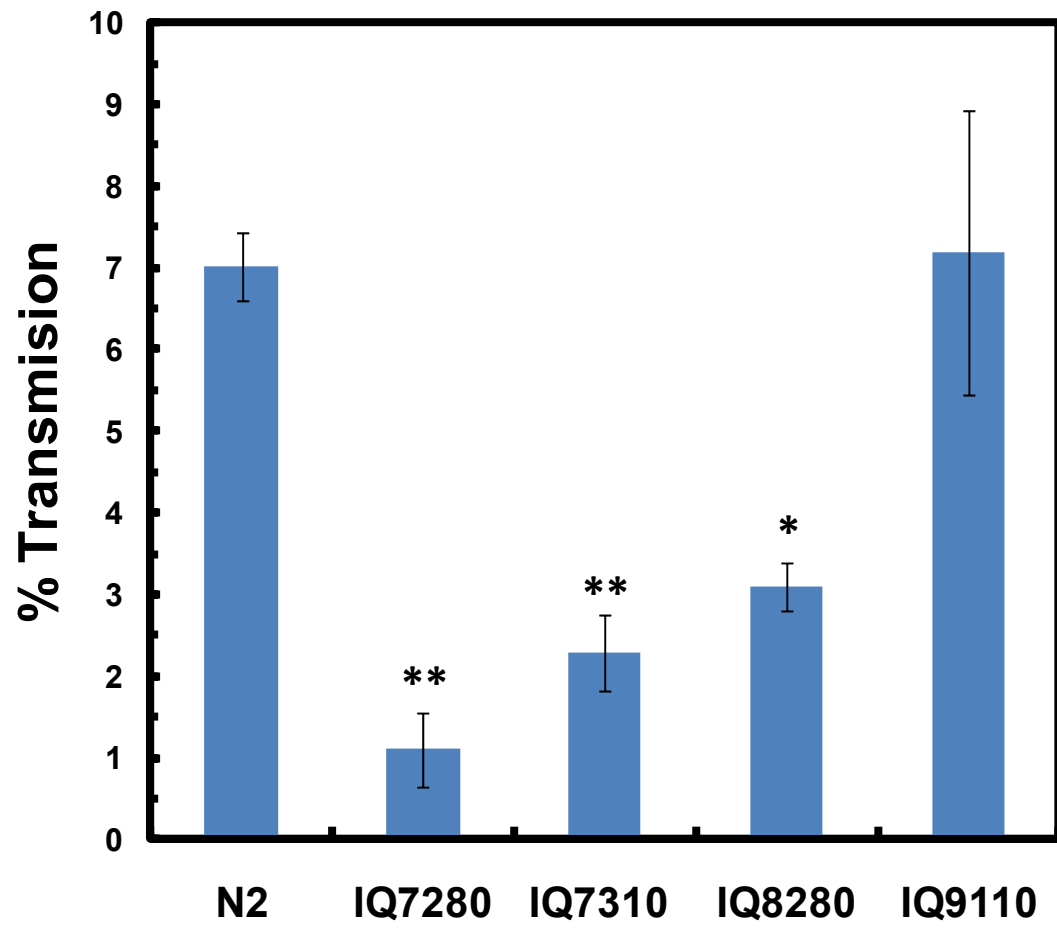
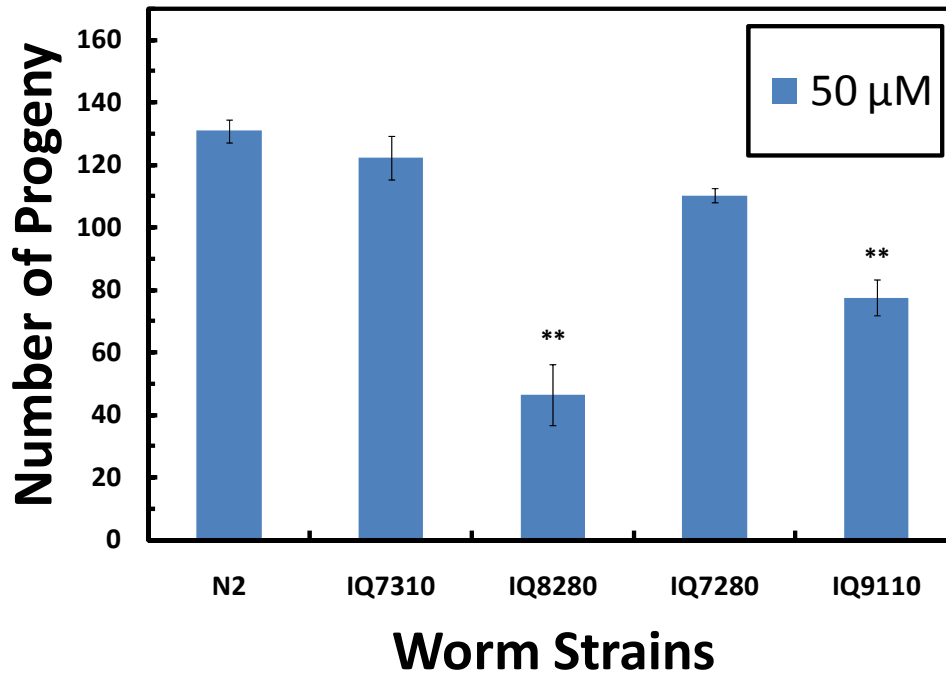


Figure 5. *them* brood size is dependent upon nutrient heme levels derived from bacteria

L4 larval stage worms of the strains indicated were grown on NGM plates seeded with *hemB* bacteria supplemented with A) 2 μ M and B) 50 μ M heme . Individual worms were transferred to new NGM plates every two days until each hermaphrodite was sperm exhausted. Brood size was determined by counting the total number of progeny laid by each individual hermaphrodite. Six hermaphrodites were used for each strain, and the data is reported as the mean \pm SEM. The * indicates $P < 0.05$ and ** indicates $P < 0.01$ to display a significant difference between *them* strains average brood size and N2 wild-type.

A



B

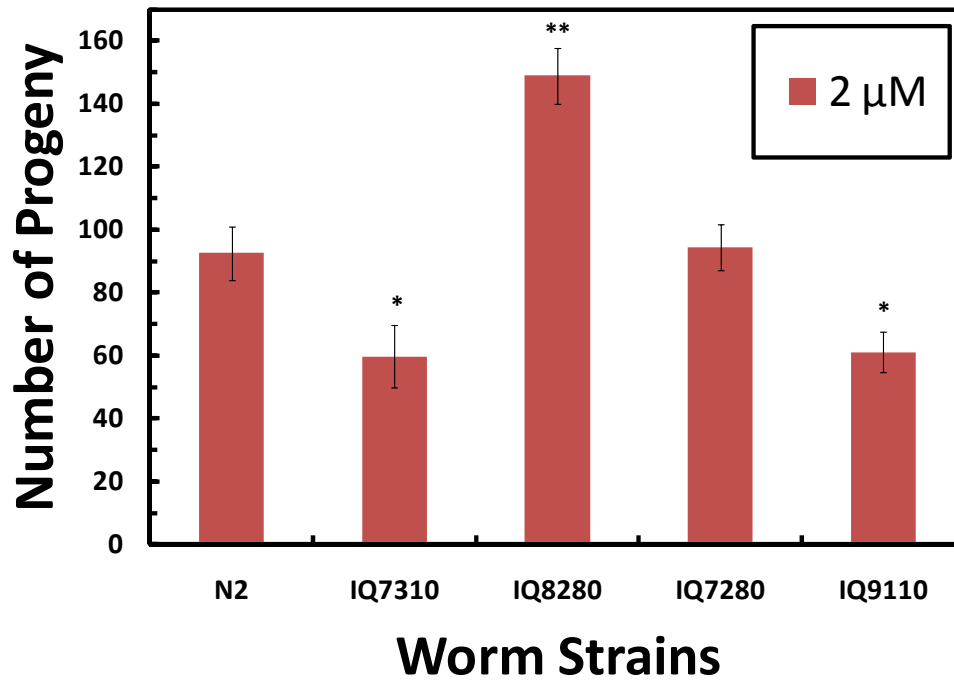
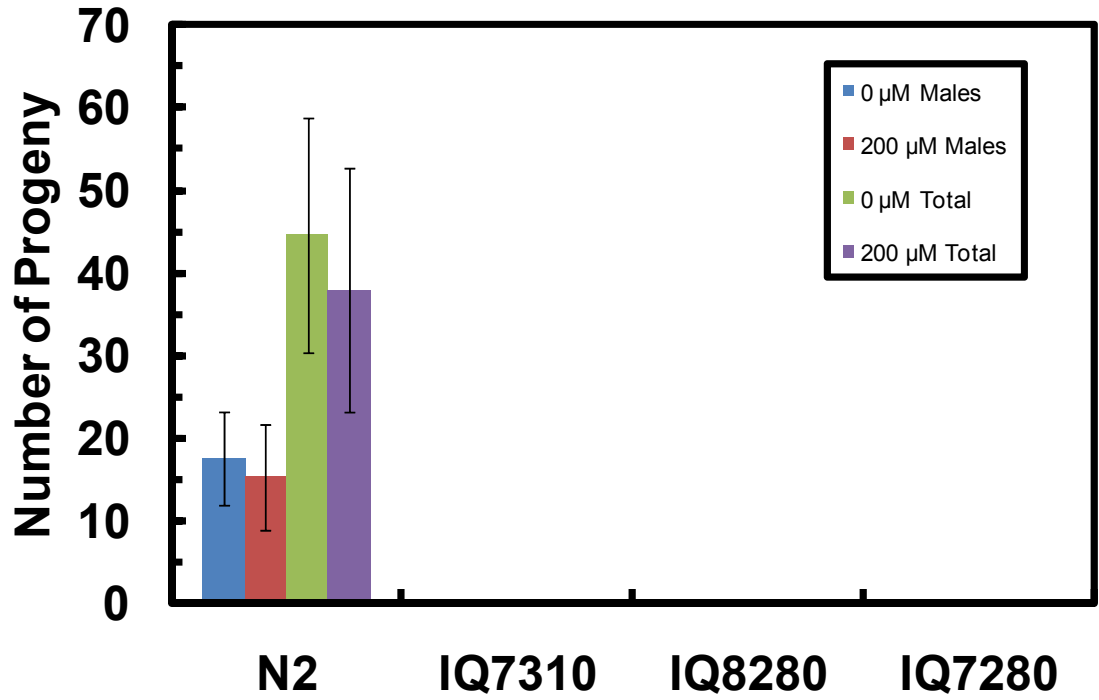


Figure 6. *them* mutants exhibit a male mating deficiency

A) N2, IQ7280, IQ7310, IQ8280 and B) N2 and IQ9110 strains were fed HT115(*DE3*) producing *him-14* dsRNAi grown in 0 μ M or 200 μ M heme. Males were crossed with BA17 (*fem-1*) hermaphrodites for 48 hours on NGM plates seeded with OP50 grown in the corresponding heme concentration. Hermaphrodites were transferred to new NGM plates seeded with OP50 grown in the corresponding heme concentration for four days at 20°C. Male progeny and the total number of progeny were counted for each hermaphrodite. The progeny from 10 hermaphrodites was analyzed, and the data is presented as the mean \pm SEM.

A



B

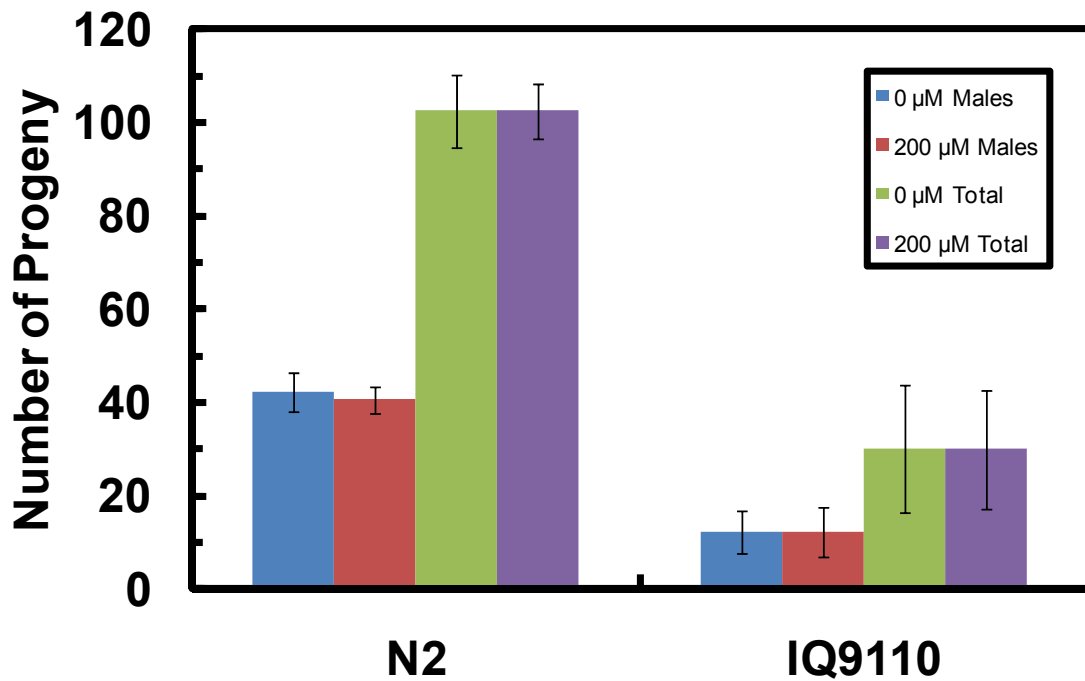
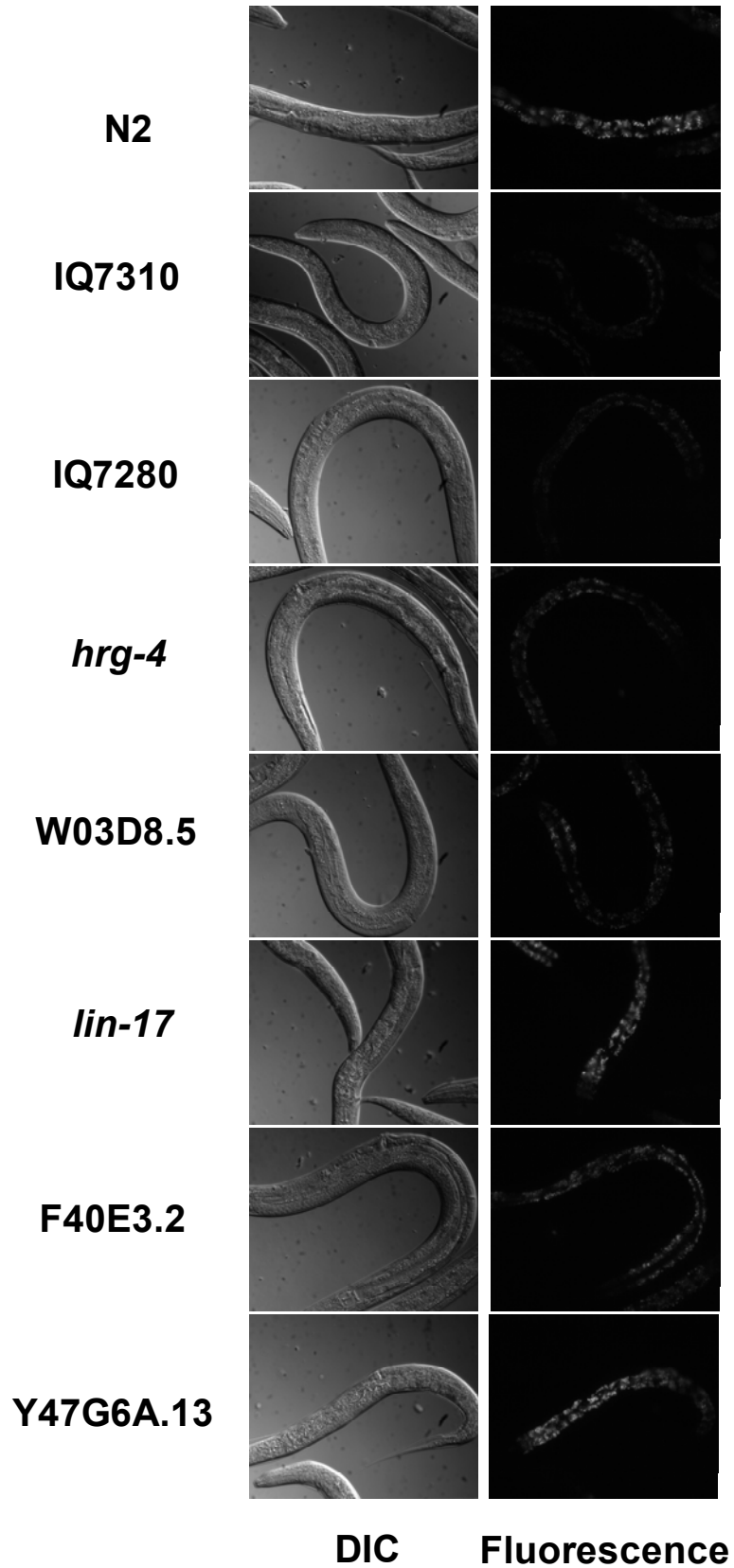


Figure 7. Reduced ZnMP uptake exhibited by *C. elegans* exposed to RNAi of candidate genes.

Candidate genes identified through genome sequencing were knocked down in N2 with RNAi for 72 hours at 15°C. ZnMP uptake in worms thus treated was compared to N2, IQ7280, IQ7310 fed HT115(*DE3*) transformed with vector and to N2 fed HT115(*DE3*) producing dsRNA targeting *hrg-4*, an intestinal heme transporter. L4 larval stage worms were incubated in mCeHR-2 media supplemented with 10 µM ZnMP and 4 µM heme at 20°C overnight. A) Representative images were acquired using a CCD camera attached to a Leica DMIRE2 epifluorescence/DIC microscope fitted with a Rhodamine filter, n=5. B) The fluorescence was quantified using Simple PCI software and the data is reported as the mean ±SEM. The * indicates P<0.05 and ** indicates P<0.01 to display a significant difference between *them* strains, RNAi treated N2 and N2 wild-type average fluorescence.

A



B

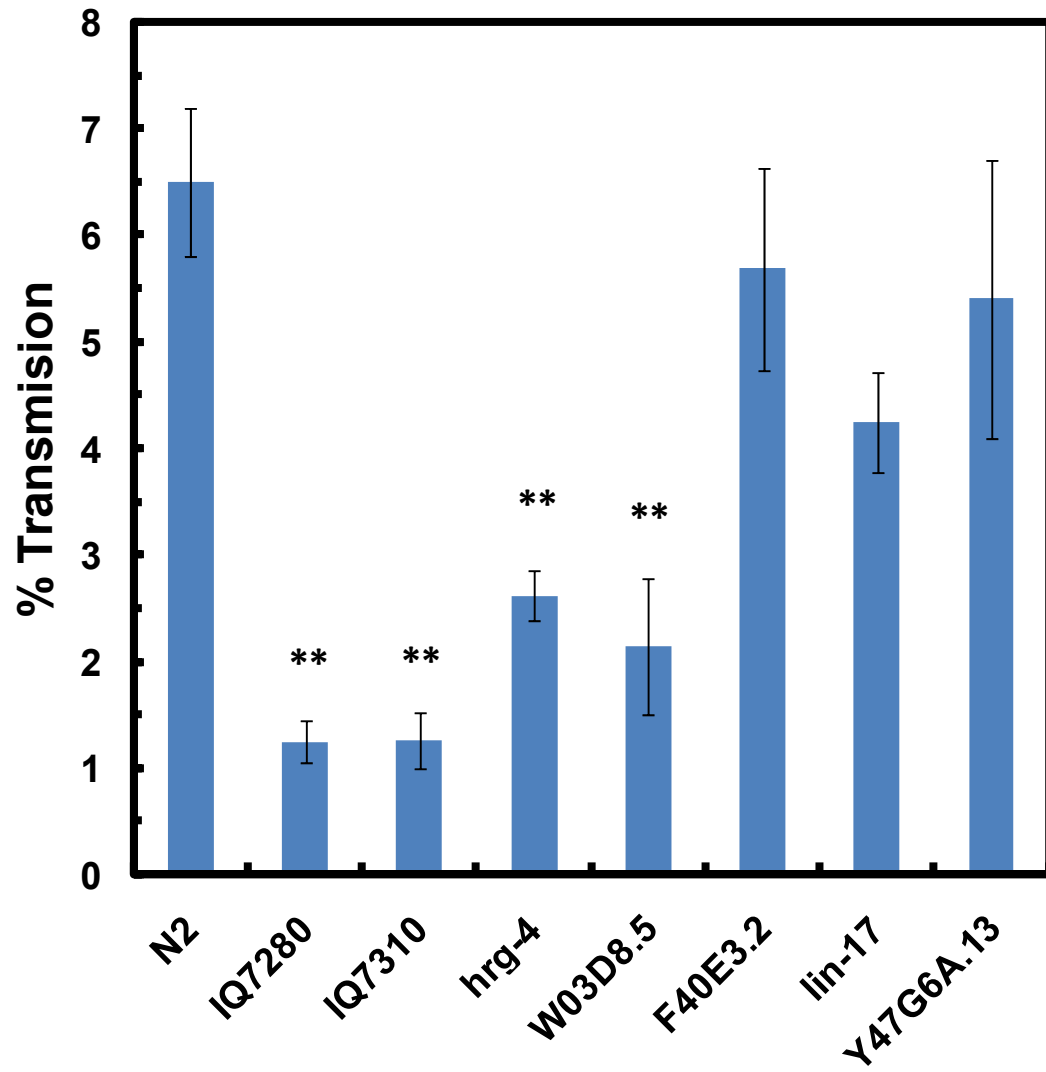


Figure 8. Rescue of *them* phenotype by microinjection of wild-type *nhr-147* in IQ9110

Individual N2, IQ9110, IQ9110/*nhr-147*, and VC1585 (*nhr-147*) L4 larval stage worms were transferred to the wells of a 96-well plate containing mCeHR-2 supplemented with 800 μ M heme. Growth of F₁ progeny was assayed by microscopy after 7 days. The number of F₁ progeny which exhibited growth beyond wild-type was divided by the total F₁ progeny in the well. Thirty wells were examined for each strain and the experiment was performed in duplicate. The data is presented as the mean \pm SEM and the * indicates significance between indicated strains, P<0.001.

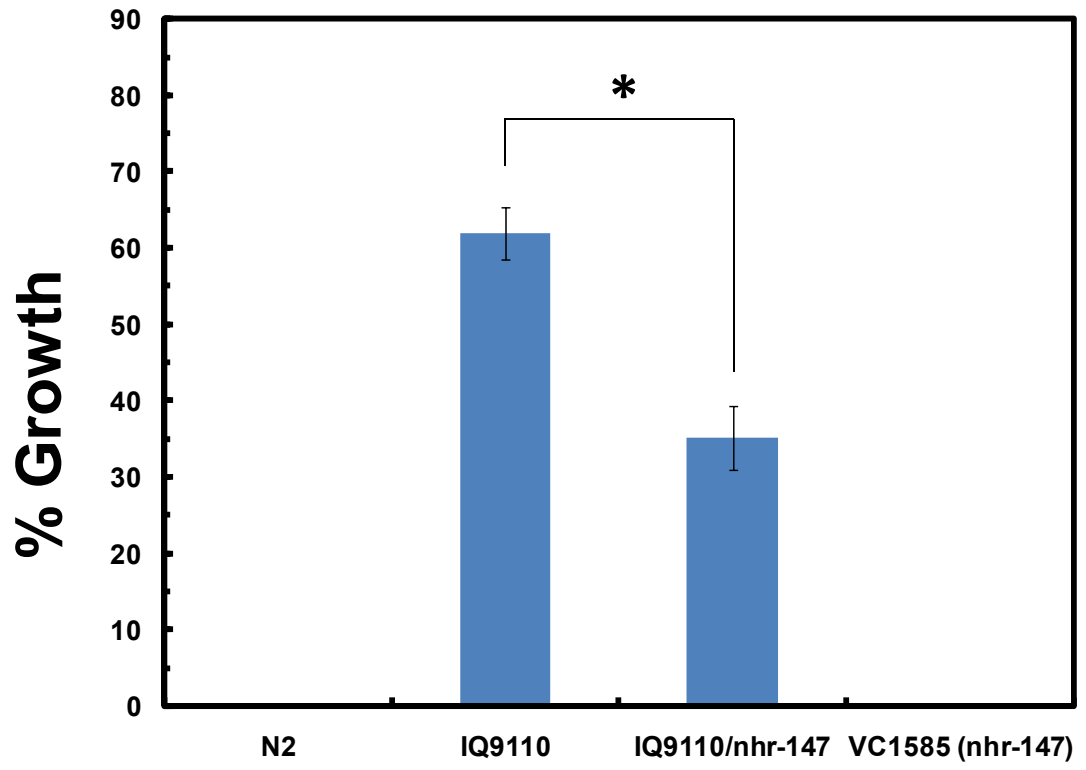


Table 1. List of SNP markers and the N2 percentage for *them* mutants on each of the six chromosomes

them strains indicated had each all six chromosomes analyzed for recombination by pyrosequencing. A SNP marker positioned in approximately the center of each chromosome was examined for the percentage of N2 SNPs. N2 SNP percentage was obtained by dividing the number of N2 SNPs by the total number of SNPs analyzed. SNPs are labeled by chromosome and genetic location in centimorgans. The following numbers of samples were used for each strain: IQ7280 n=25, IQ7310 n=24, IQ8280 n=19, and IQ9110 n=14.

% recombinant chromosomes with N2 genotype

Mutant	<i>pkP1057</i> (I) (+1.0 cM)	<i>pkP2148</i> (II) (+0.1 cM)	<i>pkP3051</i> (III) (+0.6 cM)
IQ7280	84.6	47.5	45.8
IQ7310	97.7	37	47.9
IQ8280	84.3	47.4	40
IQ9110	65.4	39.3	42.9

	<i>pk4064</i> (IV) (+0.1 cM)	<i>pkP5513</i> (V) (+0.1 cM)	<i>amP117</i>(X) (+1.4 cM)
IQ7280	50	52	76
IQ7310	41.3	45.8	62.5
IQ8280	31.6	65.8	52.8
IQ9110	70.8	100	38.5

Table 2. List of SNP markers and the N2 percentage for *them* mutants along chromosome I and V

IQ7280, IQ7310, IQ8280, and IQ9110 were analyzed to determine the genetic interval where the mutation was located. Twelve SNPs present in chromosome I were analyzed and nine SNPs on chromosome V were analyzed. N2 SNP percentage was obtained by dividing the number of N2 SNPs by the total number of SNPs analyzed. SNPs are labeled by genetic location in centimorgans. The following numbers of samples were used for each strain: IQ7280 n=25, IQ7310 n=24, IQ8280 n=19, and IQ9110 n=14.

% recombinant chromosomes with N2 genotype

Chromosome I

Mutant	<i>pkP1050</i> (-19.3 cM)	<i>pkP1103</i> (-12.5 cM)	<i>pkP1105</i> (-8.0 cM)	<i>ihP1</i> (-5.3 cM)	<i>amP108</i> (-5.2 cM)	<i>ihP2</i> (-4.5 cM)
IQ7280	65	88	92.3	100	100	95.8
IQ7310	67.5	79.2	97.8	100	97.9	100
IQ8280	87.5	94.4	94.7	100	97.2	100
	<i>ihP3</i> (-3.8 cM)	<i>ihP4</i> (-3.2 cM)	<i>pkP1057</i> (+1.0 cM)	<i>pkP1114</i> (+1.9 cM)	<i>ihP5</i> (+17.2 cM)	<i>amP23</i> (+24.3 cM)
IQ7280	91.7	84.6	84.6	73.1	64.6	63.1
IQ7310	97.9	91.6	97.7	87.5	75	76.3
IQ8280	100	86.8	84.3	71.1	60.5	50

Chromosome V

Mutant	<i>amP56</i> (-20.0 cM)	<i>pkP5092</i> (-5.2 cM)	<i>pkP5109</i> (-2.4 cM)	<i>ihP6</i> (-0.4 cM)	<i>pkP5513</i> (+0.1 cM)
IQ9110	62.5	75	82.1	87.5	100
	<i>pkP5060</i> (+0.6 cM)	<i>hw80560</i> (+1.1 cM)	<i>pkP5066</i> (+3.0 cM)	<i>amP50</i> (+25.0 cM)	
IQ9110	83.3	67.9	75	61.5	

Table 3. Two-factor recombination map and deficiency map of *them*

A) IQ7280, IQ7310, and IQ8280 were crossed with CB713 (*unc-67*), and IQ9110 was crossed with CB524 (*unc-70*) to determine the genetic distance between *them* and *unc* mutant alleles. Heterozygous F₁ *them/unc* progeny self-fertilized and F₂ progeny were placed in mCeHR-2 media supplemented with 800 μM heme to screen for *them* and *unc* phenotype. F₂ progeny were placed in three categories based on their phenotype, non-gravid, gravid with uncoordinated movement, and gravid with no uncoordinated movement. The genetic distance reported was between the alleles was determined by dividing the total number of worms which grew to gravid with uncoordinated movement by the total number of worms screened. This distance was reported in centimorgans.

B) IQ9110 was crossed to BC1283(*eT1/sDf20*) to determine if IQ9110 mutation was located between -0.9 cM and +0.6 cM through deficiency mapping. The number of worms which grew to gravid was divided by the total number of worms screened from the F₁ generation to determine if the mutation was present within the deletion region.

A

Two point recombination mapping

Cross	Non-Gravid	Gravid (unc)	Gravid (non-unc)	Total	cM
IQ7280 x CB713 <i>unc-67 (e713)</i>	198 (86.1%)	0 (0.0%)	32 (13.9%)	230	0
IQ7310 x CB713 <i>unc-67 (e713)</i>	251 (78.3%)	5 (1.6%)	64 (20.1%)	320	1.6
IQ8280 x CB713 <i>unc-67 (e713)</i>	434 (79.5%)	4 (0.7%)	108 (19.8%)	546	0.7
IQ9110 x CB524 <i>unc-70 (e524)</i>	384 (81.5%)	1 (0.25%)	86 (18.25%)	471	0.25

B

Deficiency mapping

Cross	Non-Gravid	Gravid	Total
IQ9110 x BC1283 (<i>eT1/sDf20</i>)	69 (56%)	54 (44%)	123

Table 4. List of genes analyzed in the GaPP RNAi screen

Acession Number	Gene Name	Acession Number	Gene Name	Acession Number	Gene Name
F32B5.8	<i>cpz-1</i>	M01B12.4c		W05F2.7	
F32B5.4		M01B12.5a		W05F2.2	
F32B5.2		C45E1.1b	<i>nhr-64</i>	W05F2.3	
F32B5.1		C45E1.4		W05F2.6	
Y71F9B.5b.2	<i>lin-17</i>	K09H9.4		W05F2.5	<i>fbxa-203</i>
Y71F9B.16	<i>dnj-30</i>	K09H9.8		W05F2.4a	
Y71F9B.6		K09H9.5		K03E5.3	<i>cdk-2</i>
Y71F9B.3.1	<i>yop-1</i>	K09H9.6	<i>ipd-6</i>	K03E5.2b	
Y71F9B.8		K09H9.2.2		K03E5.1	
Y71F9B.7	<i>plk-2</i>	K09H9.7		Y47G6A.12	
Y71F9B.9b.2		K09H9.1		Y47G6A.28	<i>tag-63</i>
Y71F9B.10b	<i>sop-3</i>	Y54E10A.9a & c	<i>vbh-1</i>	Y47G6A.11	<i>msh-6</i>
Y71F9B.13c		Y54E10A.6		Y47G6A.13	
Y71F9B.14		Y54E10A.5.1		Y47G6A.10	<i>spg-7</i>
W03D8.9		Y54E10A.10.2		Y47G6A.15	
W03D8.10		Y54E10A.11		Y47G6A.9	
W03D8.1		Y54E10A.12		Y47G6A.8	<i>crn-1</i>
W03D8.8		Y54E10A.13		Y47G6A.17	
W03D8.5		Y54E10A.17.2		Y47G6A.7a.1	
W03D8.6	<i>itx-1</i>	Y54E10A.4b	<i>fog-1</i>	Y47G6A.18.2	
W03D8.11		Y54E10A.14	<i>rom-5</i>	Y47G6A.6	<i>pcaf-1</i>
W10C8.2	<i>pop-1</i>	Y54E10A.15	<i>cdt-1</i>	Y47G6A.19c	
W10C8.3		Y54E10A.3		Y54E10BL.4	
W10C8.1	<i>ccb-2</i>	Y54E10A.2	<i>cogc-1</i>	Y54E10BL.5	
W10C8.4b		Y44E3B.2		Y54E10BL.3	
W10C8.6		Y44E3B.1c	<i>zip-4</i>	Y54E10BL.6	<i>mek-2</i>
Y71F9AL.11		W01B11.3	<i>nol-5</i>	Y54E10BR.4	
Y71F9AL.10		W01B11.5b		Y54E10BR.3	
Y71F9AL.12		W01B11.2	<i>sulp-6</i>	Y54E10BR.5	
Y71F9AL.13b.9	<i>rpl-1</i>	W01B11.6a.2		Y54E10BR.6	<i>rpb-6</i>
Y71F9AL.9.2		W01B11.1		Y54E10BR.2.3	
Y71F9AL.14.2		Y44E3A.2		Y54E10BR.7	<i>mod-5</i>
Y71F9AL.16	<i>arx-1</i>	Y44E3A.3		Y54E10BR.8	<i>ztf-23</i>
Y71F9AL.6		Y44E3A.4		Y54E10BR.1	
Y71F9AL.17		Y44E3A.6b		Y71F9AM.4a	<i>cogc-3</i>
Y71F9AL.5	<i>gst-43</i>	Y71F9AL.2		Y71F9AR.1	<i>bam-2</i>
Y71F9AL.4		Y71F9AL.1		Y71F9AR.2	
Y71F9AL.18.2	<i>pme-1</i>	Y71F9AM.6.1	<i>trap-1</i>	Y71F9AR.3	

Table 5. List of candidate genes from the GaPP screen with descriptions

Accession Number	Gene Name	Description obtained from WormBase
W03D8.1		Mannosylated cell wall protein ortholog
K09H9.2.2		Sister chromatid cohesion protein ortholog
K09H9.8		Unknown
W01B11.3	<i>nol-5</i>	Ribosome biogenesis protein
Y47G6A.5		MAPKKK ortholog, controls cell integrity
Y47G6A.18.2		Golgi protein
Y47G6A.15		Isoform 5 of sarcolemmal membrane associated protein ortholog
Y47G6A.10	<i>spg-7</i>	Metalloprotease orthologous to human paraplegin
Y54E10A.15	<i>cdt-1</i>	Ortholog of replication licensing factor
Y54E10BR.6	<i>rpb-7</i>	RNA polymerase II ortholog
Y71F9AL.13b.9	<i>rpl-1</i>	Ribosomal protein, Large subunit
Y54E10A.10.2		Protein required for biogenesis of the 60s subunit of ribosomes
Y47G6A.7b.2		Predicted integral membrane protein, putative nucleotide sugar transporter
Y71F9AM.6	<i>trap-1</i>	Translocon-associated complex TRAP, alpha subunit
W03D8.9		Unknown
Y47G6A.19		Ortholog of human metallopeptidase A and B precursors
W10C8.6		Ortholog of integral membrane protein localized to vacuolar vesicles in yeast
Y54E10A.4	<i>fog-1</i>	Cytoplasmic polyadenylation element binding (CPEB) protein required for specification of the sperm fate.
Y54E10BR.3		Predicted E3 ubiquitin ligase

Table 6. Candidate genes with mutations identified through Solexa deep sequencing

<i>them</i> line	Accession Number	Gene Name	Position	Mutation	Confirmation	ZnMP	GaPP
IQ7280	F40E3.2		I: 2643611	Met->Ile	YES	-	-
	Y71F9B.5	<i>lin-17</i>	I: 2713977	Gly->Glu	YES	-	-
	Y47G6A.13		I: 3440845	Gly->Glu	YES	-	-
	Y71F9AL.4		I: 2905523	T->A	NO	N/A	N/A
IQ7310	F40E3.2		I: 2643611	Met->Ile	YES	-	-
	W03D8.5		I: 2817273	Glu->Lys	YES	+	-
IQ8280	W03D8.5		I: 2816636	none (5' UTR)	NO	+	-
IQ9110	K09H11.11		V: 5755526	Lys->Gln	YES	N/A	N/A
	W06H8.1	<i>ttn-1</i>	V: 6125876	Phe->Leu	YES	N/A	N/A
	C03G6.8	<i>nhr-147</i>	V: 7347869	Gly->Cys	YES	N/A	N/A
	K11G9.4	<i>egl-46</i>	V: 6680373	Lys->Glu	NO	N/A	N/A
Background Mutations	Y39G10AR.17		I: 2379643	Met->Ile	YES	N/A	N/A
	C54F6.14	<i>ftn-1</i>	V: 7546600	His->Tyr	YES	N/A	N/A

Chapter 4: Discussion

Delineating the intracellular network which regulates heme homeostasis has been difficult because of the inability to experimentally uncouple heme biosynthesis from heme trafficking. The Hamza laboratory determined that *C. elegans* is a unique animal model for interrogating the heme trafficking pathways, as it lacks the entire heme biosynthesis pathway and is therefore a natural heme auxotroph (14). Since *C. elegans* acquires heme solely from the environment, it must contain uptake and trafficking pathways for distributing heme to various tissues, cells, and organelles (36). Unlike other model organisms which synthesize endogenous heme, *C. elegans* is dependent on exogenous heme, thereby providing us with the unique opportunity to control internal heme levels within an organism completely through dietary sources.

Heme is essential for *C. elegans* growth and survival, yet excess levels can be toxic. Wild-type *C. elegans* grown at heme concentrations $<1.5 \mu\text{M}$ or $\geq 800 \mu\text{M}$ in liquid mCeHR-2 media become growth arrested. Although growth arrested worms from $<1.5 \mu\text{M}$ can be transferred to $20 \mu\text{M}$ heme and they recover; worms grown at $800 \mu\text{M}$ do not. We speculate that worms grown at toxic heme concentrations are irreversibly growth arrested due to the cytotoxicity associated with free heme. To identify genes involved in heme homeostasis in *C. elegans*, Dr. Anita Rao, a former postdoctoral researcher in the Hamza laboratory, performed a mutagenesis screen to generate mutants which could grow and reproduce at $800 \mu\text{M}$ heme in axenic liquid growth medium. This novel screen was the first to create mutant *C. elegans* strains with phenotypes related to heme homeostasis. Thirteen mutant strains were identified and termed toxic heme resistant mutants (*them*). Since *them* mutants were isolated from CeHR-2 axenic liquid cultures

and the phenotype was only visible in liquid medium, traditional, well-established genetic mapping techniques that were designed for *C. elegans* mutants isolated from NGM agar plates were not easily applicable to map *them* mutations.

Attempts to localize *them* mutations using established protocols were met with a variety of technical challenges. Dr. Rao attempted to use restriction fragment length polymorphism mapping on sample *them* strains from five unique complementation groups (Appendix C). This technique was unsuccessful since she was unable to determine on which chromosome *them* mutations were localized for any of the *them* strains. While working as an undergraduate research assistant, I attempted to use three-factor recombination mapping with strains MT464 and MT465, which also produced inconclusive data for determining on which chromosome *them* mutations were located. Each *them* strain had been generally characterized with complementation mapping, segregation, growth curves, and resistance to heme analogs in liquid culture; however, it seemed doubtful that the mutated gene would be identified since we were unable to pinpoint *them* mutations to a specific chromosome.

Fortunately, next generation sequencing technology provided the opportunity to identify the location of the mutations responsible for *them* phenotypes. A previous study showed that mutations which caused dietary zinc resistance could be mapped in *C. elegans* using SNPs and pyrosequencing (65). Therefore, we adopted pyrosequencing for our purposes, using techniques established by the Kornfeld laboratory at Washington University, St. Louis.

Pyrosequencing provided a rapid method to analyze the genomes of the *them* strains for identification of the approximate position of *them* mutations. Three-factor

recombination mapping can often take weeks to determine the location of a specific mutation on a chromosome. Through the use of pyrosequencing, recombination frequencies can be analyzed in a few hours. This method is limited only by the time spent designing primers necessary for analyzing a particular SNP marker. Using this technique, we were able to identify the chromosome and genetic interval where *them* mutations mapped. The pyrosequencing mapping was confirmed with both two-factor recombination mapping and deficiency mapping.

Once the genetic interval, which contains 114 genes, had been located, it was necessary to identify a method suitable for analyzing genes within this region. The most common method used in *C. elegans* to analyze genes on a large scale is RNAi (80). RNAi can be performed through microinjection and soaking with dsRNA, both of which are expensive and time consuming methods for screening large numbers of genes in *C. elegans*. Another method to perform RNAi is by feeding dsRNA producing HT115(*DE3*) bacteria; however, this method can only be successfully performed on NGM agar plates, a growth medium on which there is no heme resistant phenotype. This led us to identify phenotypes associated with *them* mutants that are easily detected on agar plates and which can be used in a discernable manner to conduct precise genetic mapping.

IQ7280, IQ7310, and IQ8280 exhibited resistance to the toxic heme analog GaPP on plates when compared to wild-type. These strains also displayed reduced fluorescent heme analog uptake of ZnMP after being grown on plates when compared to wild-type. Both of these phenotypes could be due to a defect in heme transport or a regulatory mechanism such as a transcription factor or signaling pathway which controls

heme transport. When grown on *E. coli hemB* bacteria supplemented with high heme, IQ8280 and IQ9110 both exhibited a reduced brood size. Worms which were fed heme deficient diets on plates resulted in a significantly increased brood size in IQ8280, while IQ7310 and IQ9110 produced brood sizes that were significantly reduced from wild-type. It appears that IQ7310 and IQ8280 are affected by the concentrations of heme on plates. IQ7310 exhibits a phenotype that corresponds to a defect in heme transport, whereas IQ8280 exhibits a phenotype that corresponds to a defect in heme degradation or recycling. Additionally, IQ7280, IQ7310, and IQ8280 males were unable to mate successfully. While this could be a defect in sperm production or mating structures, observation of mating behaviors leads us to believe that *them* males lack the ability to identify hermaphrodites for mating. Based on these phenotypes, we decided to use the GaPP toxicity assay because it appeared to be reasonably robust. The screen identified 19 candidate genes exhibiting GaPP resistance when depleted, an unusually large number.

As sequencing technology has advanced, so has its cost effectiveness. Sequencing the entire genome of mutant organisms has currently become an economically feasible technique. To identify the mutations within the genetic interval mapped by pyrosequencing, the Solexa/Illumina deep sequencing platform was used to sequence the entire genomes of IQ7280, IQ7310, IQ8280, and IQ9110 *them* mutants. Although, sequencing the entire genomes of these four mutants was completed in five days, analyzing the genetic data required more than a month. Unfortunately, none of the genes which contained mutations from the genome sequencing were within the 19 genes identified in the GaPP RNAi screen. This is possibly due to GaPPs indiscriminate

disruption of proteins. Any protein which interacts with heme will lose its function when exposed to GaPP, this indicates massive cytotoxicity will occur when GaPP is absorbed. This makes it difficult to pinpoint which gene is actually responsible for the *them* phenotype.

Once the Solexa sequencing results had been confirmed with directed Sanger DNA sequencing, the mutations were verified using RNAi in wild-type N2 strain to determine if any of these genes were responsible for phenotypes exhibited by *them* strains. The only candidate gene which displayed a *them* phenotype was W03D8.5. The mutation present in W03D8.5 was a glutamic acid to lysine amino acid change and was the only mutation in IQ7310 within the genetic interval mapped by pyrosequencing. When W03D8.5 was knocked down, reduced ZnMP fluorescence was observed in the worm intestine, however no morphological or reproductive related phenotypes have been observed. The function of W03D8.5 is unknown; however, a putative function could be ascertained since it contains a major sperm protein (MSP)-like domain and a Pap-D like domain. It is unclear how a MSP is involved in heme homeostasis, however, a mutant deficient in this protein could be relatively sterile. This would explain the male mating defects in IQ7310. The PapD-like domain is a motif that is found in pathogenic bacterial periplasmic chaperones involved in assembling adhesive surface organelles used to infect its host (81). Therefore this protein may play an indirect role in heme homeostasis by assembling other proteins involved in trafficking or uptake. Unfortunately, when this gene was examined by RNAi for GaPP resistance, we did not find any significant resistance when compared to wild-type. A rescue experiment using wild-type W03D8.5 injected into IQ7310 would be necessary to confirm W03D8.5's role in IQ7310 *them*

phenotype. As a result of these findings, we were unable to confidently conclude whether this mutation was responsible for IQ7310 phenotype.

IQ9110 contains a mutation in *nhr-146* that we were able to partly rescue by analyzing toxicity at high heme. Surprisingly, an *nhr-147* deletion strain, VC1585, is not resistant to toxic concentrations of heme. Since VC1585 has a deletion in the N-terminus of *nhr-147*, the entire DNA binding domain and a portion of the ligand binding domain has been disrupted. The mutation in IQ9110 is a substitution of glycine with cysteine and in close proximity to the ligand binding domain containing a CXC motif. Therefore, the IQ9110 mutation may disrupt the secondary or tertiary structure of NHR-147 sufficient to prevent heme/ligand binding but not DNA binding. By contrast, a *nhr-147* deletion mutant is a null mutant and will lack both activities and may show a more severe phenotype. Previous studies have identified a mammalian nuclear hormone receptor, REV-ERB α , which binds heme to regulate genes involved in the circadian rhythm (34). When heme binds REV-ERB α , this causes transcriptional repression of its target genes. It is possible that *nhr-147* functions in the same manner, repressing its target genes when bound to heme.

The function of *nhr-147* in *C. elegans* is currently unknown. RNAi experiments have not displayed any morphological or reproductive phenotypes in N2 wild-type worms. The only allelic strain present is VC1585 which has exhibited no heme resistance. However, NHR-147 which shows >47 % identity at the amino acid level was identified in a genome wide RNAi screen using a *C. elegans* heme sensor strain (Hamza, personal correspondence). Within NHR-147 and NHR-149, there is a stretch of 16 amino acids which contains the CXC motif preceding the residue which contains glycine to

cysteine mutation (Fig. 1). While *nhr-147* is an exciting candidate, more work must be performed to confirm whether the cysteine mutation is responsible for the IQ9110 strain *them* phenotype. Deficiency mapping must be utilized to determine whether the mutation in *nhr-147* conveys heme resistance. Identifying downstream target genes of *nhr-147* may elucidate the regulatory subnetwork which maintains heme homeostasis within *C. elegans*.

An interesting mutation of a histidine to tyrosine conversion within *ferritin-1* (*ftn-1*) was identified in all four strains. This is a protein that stores iron and releases it in a controlled manner when required by the cell. Stocks from the original N2 strain received from the CGC were thawed out and DNA was extracted for sequencing. The *ftn-1* mutation was also identified in the N2 wild-type strain, which leads us to believe this mutation does not contribute to the *them* phenotype. Another mutation which appeared in two *them* strains, IQ7280 and IQ7310, was a methionine to isoleucine conversion in F40E3.2. It is possible that two mutations are required for the *them* phenotype in these strains. It may be possible that a combination of F40E3.2 and W03D8.5 mutations work together to disrupt heme homeostasis sufficiently so as to lead to heme resistance in strain IQ7310. This could be tested by coinjecting dsRNA targeting both, F40E3.2 and W03D8.5, and screening for heme resistance.

While we were unable to confirm which mutation was responsible for toxic heme resistant phenotype for each of *them* strains, the project of mapping *them* has been an evolving process, especially since these were the first mutants produced with a phenotype which is observed only in axenic liquid media, a characteristic which requires extensive standardization for genetic mapping. Next generation sequencing technology coupled

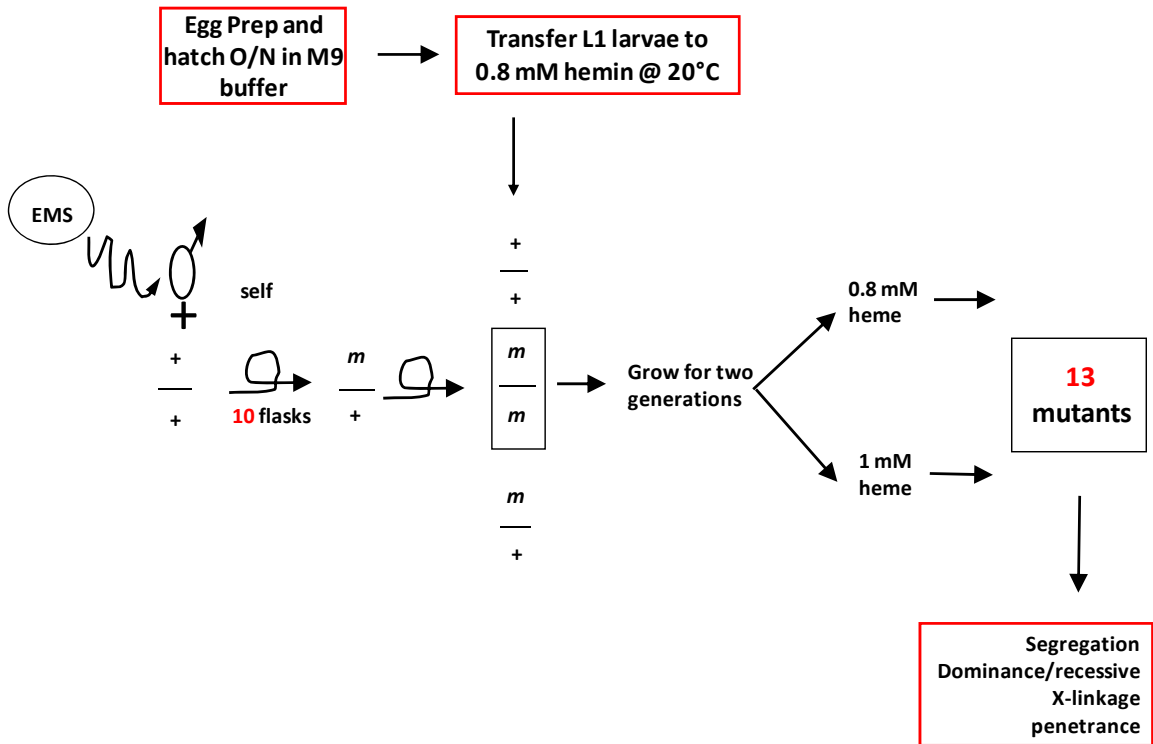
with SNP mapping using pyrosequencing has been able to provide alternative methods for identifying mutations. Future studies aimed at delineating the role of the possible candidate genes in Table 6, and *nhr-147* in organismal heme homeostasis, will greatly increase our understanding of eukaryotic heme regulation and trafficking.

Figure 1. Homologous amino acid sequence between *nhr-147* and *nhr-149*

The amino acid sequence of *nhr-147* and *nhr-149* were aligned using ClustalW and Boxshade 3.2.1. The IQ9110 mutation of glycine to cysteine mutation is highlighted in red. The conserved region around the mutation is indicated by a red box. Conserved amino acids are highlighted in black and amino acids with similar charge or polarity are indicated highlighted in grey. Below the two aligned amino acid sequences is the consensus notation, which uses * to indicate identical amino acids.

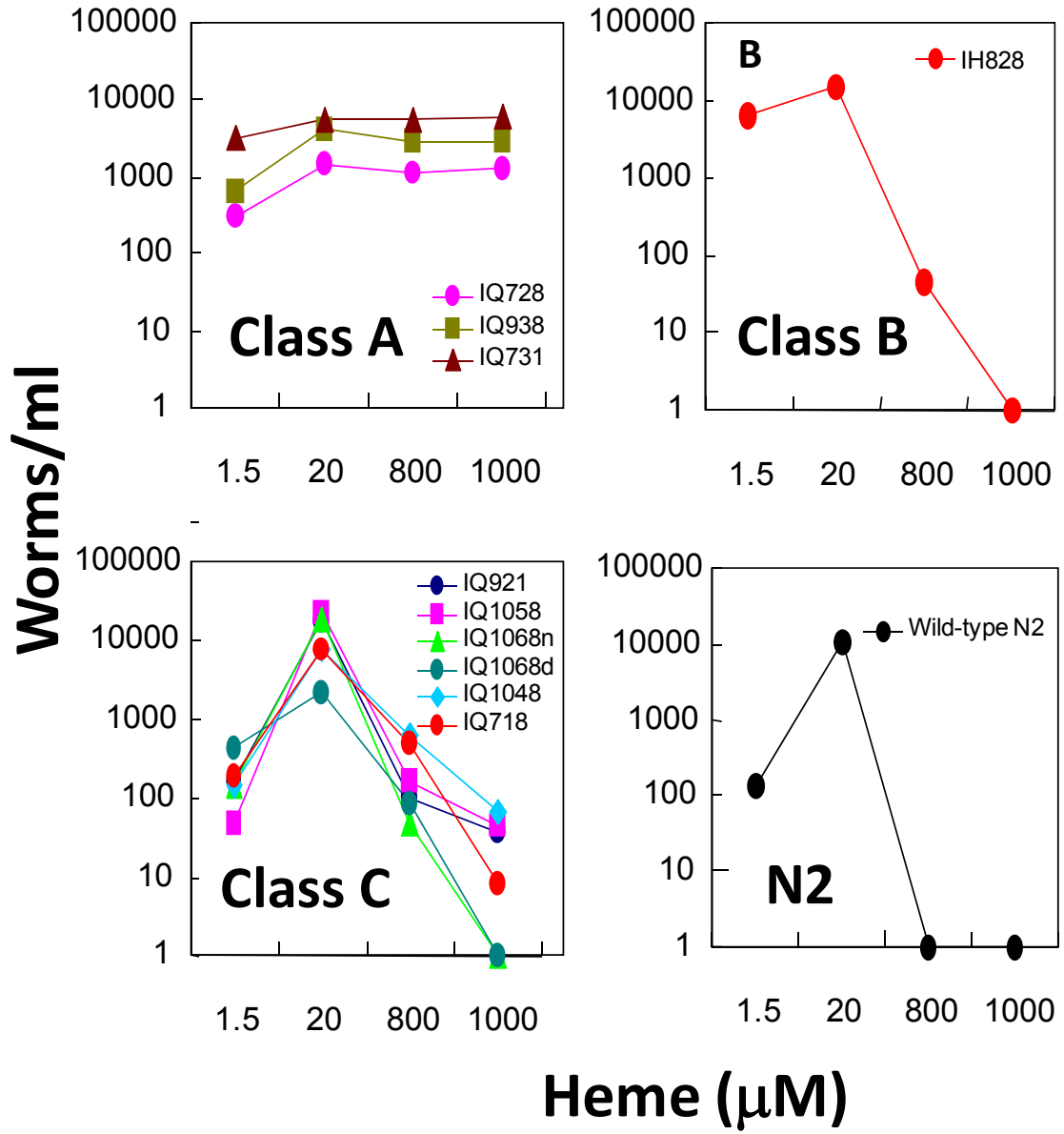
Appendix A: Toxic heme resistance mutagenesis screen design

Wild-type N2 hermaphrodites were exposed to methylsulfonic acid, ethyl ester, in mCeHR medium. Worms self-fertilized and produced F₁ heterozygous progeny. F₁ progeny were synchronized and F₂ L1 larval stage worms were exposed to mCeHR supplemented with 800 μM heme. Strains which exhibited growth at 800 μM heme were grown for two generations and exposed to mCeHR supplemented with 800 μM or 1 mM heme. From this screen 13 mutants were identified. This screen was conducted by Dr. Anita Rao.



Appendix B: Heme dependent growth curves of *them* and resulting phenotypic clusters

N2 wild-type and thirteen *them* strains were grown in mCeHR-2 media supplemented with 1.5 μM , 20 μM , 800 μM , and 1 mM heme. Based upon *them* growth curves, strains were placed in three phenotypic clusters: class A, class B, and class C. Figure provided by Dr. Anita Rao.



Appendix C: List of thirteen *them* strains organized into five complementation groups and three phenotypic clusters

Strain	Complementation Group	Phenotypic Cluster
IQ7280	1	A
IQ9380	1	C
IQ9680	1	C
IQ7310	2	A
IQ9210	2	C
IQ7180	2	C
IQ8280	3	B
IQ1068d	4	C
IQ1068	4	C
IQ1048	4	C
IQ1058	4	C
IQ1031	4	C
IQ9110	5	C

Appendix D: List of primers used in pyrosequencing

Primer Name	Sequence
5_K04F10 Ch. 1 0.95	AGC GCT GCT CCG GTT CAT AGA TTC CTC TGT GGT CTT CTG GCT TGA TT
3_K04F10 Ch. 1 0.95	ATT TCA GGA AAG CCG ACT GG
Seq_K04F10 Ch. 1 0.95	CCA TAC TGA TCA CGT CAT
amp17(B)-Left	AGC GCT GCT CCG GTT CAT AGA TTA ATG CAT GAG GGA TGG AGA A
amp17(B)-Right	GGT GCG AAT ATG AAA AAC TCG
amp17(B)-Seq	CCA GAT CAT CAA TTT A
5_F49B2	AGC GCT GCT CCG GTT CAT AGA TTC TCG TAG TTT GCA CTC CCT CTC
3_F49B2	GAA GAG CAA TAA GGG GCA AA
Seq_F49B2	TGC CCA AGA CGT AAA
amp23-Left	AGC GCT GCT CCG GTT CAT AGA TTT CGT AGT TTG CAC TCC CTC TC
amp23-Right	GAA GAG CAA TAA GGG GCA AA
amp23-Seq	TGC CCA AGA CGT AAA
5_F56C11	AGC GCT GCT CCG GTT CAT AGA AAG AGG ATC TGG AGC AGA AGT T
3_F56C11	GTA GGA GTT CGA CAA TCG TGA AAT T
Seq_F56C11	CCA GAT CAT CAA TTT A
5_Ch1 y71g12a(-12.41)	AGC GCT GCT CCG GTT CAT AGA TTC ACC TAG AAT AAG AAT GGG CAG G
3_Ch1 y71g12a(-12.41)	TTT GGC TTA TTG CCG ATA TGC
Seq_Ch1 y71g12a(-12.41)	CCG CCC ACC CCT AGA
Chly47g6A(-3.19)_fwd	AGC GCT GCT CCG GTT CAT AGA TTG CGC GTG AAA TAT GAT GTA TTG A
Chly47g6A(-3.19)_rev	CGC TGG TAG CTC CAA AAA TAA T
Chly47g6A(-3.19)_seq	ATA CAT TGG GAT GAT GG
5_Ch1 f21c3(2.0)	AGC GCT GCT CCG GTT CAT AGA TTC AGA TTG AGG CTG AAA TAT GGT G
3_Ch1 f21c3(2.0)	GTC GAG CAG CAC CAG TTA TTG
Seq_Ch1 f21c3(2.0)	CAA CGA TGC TTC AAC TG
5_Ch1 y26d4a(17.2)	AGC GCT GCT CCG GTT CAT AGA TTC GCG ACG CAA TTC TTC CTA TG
3_Ch1 y26d4a(17.2)	CGC CAA AAT TGG TCA GTT GG
Seq_Ch1 y26d4a(17.2)	TTC GTT GAA ATC GTG
5_Ch1 F32B5(-8.11)	AGC GCT GCT CCG GTT CAT AGA TTC TAA TGT ACC ACC TCA CGT GAC G
3_Ch1 F32B5(-8.11)	CTT TCA CCA GAA CCC TCT ATT C
Seq_Ch1 F32B5(-8.11)	CGC AGT TTT TCA ATT TGT
5_Y54e2a Ch 2 Right	AGC GCT GCT CCG GTT CAT AGA TTC CGA ACA AGC CTA CAA GAC CA
3_Y54e2a Ch 2 Right	TTA GTA GAT GTA GCG GGG TT
Seq_Y54e2a Ch 2 Right	CCA CGA GCA TCA AAA T
5_F37H8 Ch 2 +3.34	AGC GCT GCT CCG GTT CAT AGA TTC TTT ATT AAT GGA GCC CCA GGT
3_F37H8 Ch 2 +3.34	TTG TAT CAA AAG ATC GTA GTG AAA
Seq_F37H8 Ch 2 +3.34	CAA AAG ATC GTA GTG AAA AA
5_ZK1098 Ch 3 Center	AGC GCT GCT CCG GTT CAT AGA TTC AGA TGC AGG AGC AAA TTA CGA
3_ZK1098 Ch 3 Center	TGG AAT CTA GGG CAC TCT TTT T
Seq_ZK1098 Ch 3 Center	CAT GAG GAG GAG ATT AAG AC
5_Ch3 Center	AGA TGC AGG AGC AAA TTA CGA
3_Ch3 Center	TTT TTC TCA CGG GAT CTA AGG TTT AGA TAC TTG GCC TCG TCG CGA
Seq_Ch3 Center	CAT GAG GAG GAG ATT AAG AC
5_Ch4 CenterFWD	AGC GCT GCT CCG GTT CAT AGA TTG TGG AGC ATG TCA ATT CTG AAA
3_Ch4 CenterREV	AGC GCT GCT CCG GTT CAT AGA TT
Seq_Ch4 CenterSEQ	AAA CGG GTT TCA TAC TG
5_Ch. 6 CENTER T25B6	AGC GCT GCT CCG GTT CAT AGA TTG CGA CGC AAT TCT TCC TAT G
3_Ch. 6 CENTER T25B6	CGC CAA AAT TGG TCA GTT GG
Seq_Ch. 6 CENTER T25B6	TTC GTTG AAA TCG TG

Appendix D continued

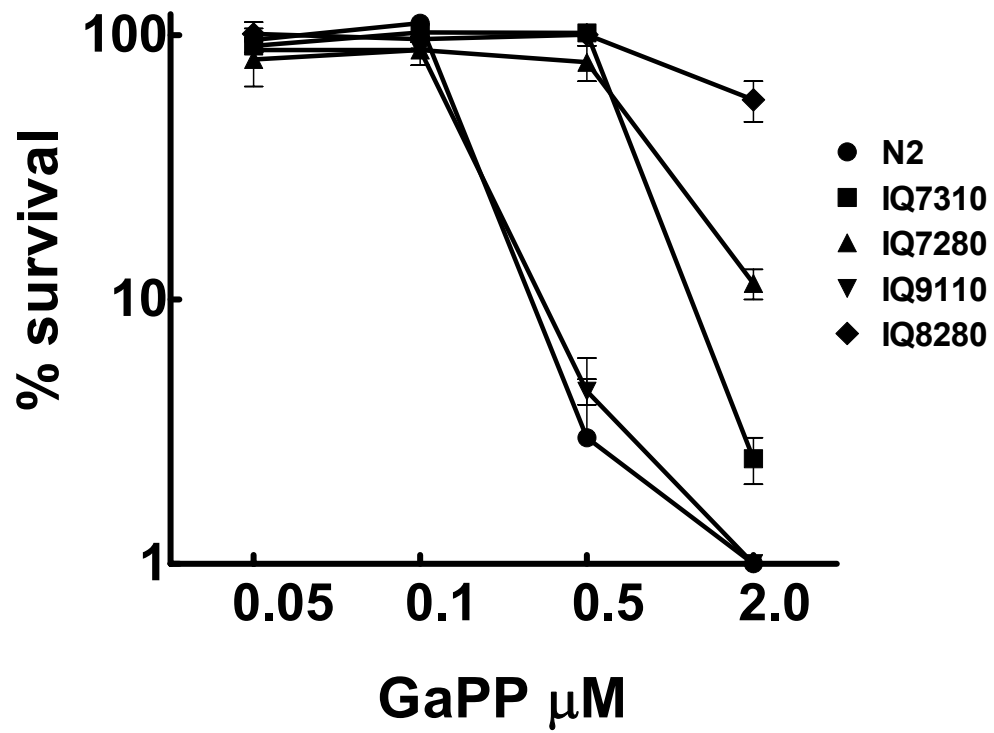
Primer Name	Sequence
5_Ch5 CENTER F44C4	CGG GAA CCT GAC TCT TCT ATT G
3_Ch5 CENTER F44C4	TCT CGA GAA AAT TGC TGA TG
Seq_Ch5 CENTER F44C4	CAG GAT GTT TGG GCG
5_F44C4 Ch5 Center FW	GCC AGA TAG TGA CGA TTG TTG A
3_F44C4 Ch5 Center RE	AGC GCT GCT CCG GTT CAT AGA TTG GAA GAA GGG AAT TTG AAA TAA
Seq_F44C4 Ch5 Center SE	CAC TGG ACT ATC GTC GA
5_ZC15 Ch5 amp50- Left	AAA TTG CAC TTT GGG GGA TT
3_ZC15 Ch5 amp50- Right	AGC GCT GCT CCG GTT CAT AGA TTG GGC GAT GAT GAA CAG AGA G
Seq_ZC15 Ch5 amp50- Seq	TTT TCT TCA TTC TTT CCA
5_R01B10	AGC GCT GCT CCG GTT CAT AGA TTG GTG TCA TGT GTT CAT GCA GCT AA
3_R01B10	AGC GCT GCT CCG GTT CAT AGA TT
Seq_R01B10	GAC CCT CAT TCT TCA TTT
5_T01C4	AGC GCT GCT CCG GTT CAT AGA TT
3_T01C4	AGC GCT GCT CCG GTT CAT AGA TTA AGA AGATAT CCC GAT TAA CAA ACG
Seq_T01C4	AAC AAA CGG ATG ACG
5_Ch.X Center -FWD	AGC GCT GCT CCG GTT CAT AGA TTG CAT AGC AAC TAT TGC CCA AA
3_Ch.XCenter -REV	TTT TTC GAT GTT TCG CAC AG
seq_Ch.X Center	ATG CAC TTA GCC GGA
5_Ch.X +6.8_F1	AAG TGC TTG CCG GAG TAGAGG
3_Ch.X +6.8_R2	AGC GCT GCT CCG GTT CAT AGA TTG CGA AACAAA CCT GGG TGA CG
Seq_Ch.X +6.8_S1	TGT CTC CAC GCG AAT
5_CHX FL F02G3	AGC GCT GCT CCG GTT CAT AGA TTT CTG AAA TCG TGT TGC GAA GTC
3_CHX FL F02G3	TCT TCA GTT GGT TAA GGT CCT C
Seq_CHX FL F02G3	TCT TCC AGT TGG TTA AGG CCT CT
5_CHX (-1.89) B0403	AGC GCT GCT CCG GTT CAT AGA TTG AAC CTC CAA CTT CGA AGG AC
3_CHX (-1.89) B0403	CAA GAC TAC GAT GGA GGA CG
Seq_CHX (-1.89) B0403	AAC ATG CCA GCT CCA
5_ChX 1.88 C32A9	AGC GCT GCT CCG GTT CAT AGA TTA AAC GTG AGG CAG CTA ACT AC
3_ChX 1.88 C32A9	AAA CGA GCA AAG TGC GTG TG
Seq_ChX 1.88 C32A9	GGA ATG TTC TGA AAA ATA AT
5_CHX FR C16H3	AGC GCT GCT CCG GTT CAT AGA TTG CGA TGC GGT TTC CTA GCT TAC
3_CHX FR C16H3	ATT GCC CAT TTC AAG CCC
Seq_CHX FR C16H3	CCA TCA TCT GAT AC
5_Ch1 w10c8(-5.39)	AGC GCT GCT CCG GTT CAT AGA TTA CTA CTT TCC CAT GTT TCG ACA CT
3_Ch1 w10c8(-5.39)	CCG CTT TCG TCA ATG ATG G
Seq_Ch1 w10c8(-5.39)	CGG TTT ACC GGT GTG
5_-5.2Y54E10BL	AGC GCT GCT CCG GTT CAT AGA TTC CAG GAC GAG CTT CGT GAT TG
3_-5.2Y54E10BL	GCC GTC AGT CCG ACA ACA GAT C
Seq_-5.2Y54E10BL	CAT CGG CAG AGC CAG
Ch1_c45e1_fwd	AGC GCT GCT CCG GTT CAT AGA TTC ATC CAT ACA AAT GCG CTC TAC T
Ch1_c45e1_rev	CCG AAG AAG TGG TAC TTA TAC GC
Ch1_c45e1_seq	CAG GAT GTT TGG GCG
5_W05F2 (-3.82)	AGC GCT GCT CCG GTT CAT AGA TTA CTA CTT TCC CAT GTT TCG ACA CT
3_W05F2 (-3.82)	CCG CTT TCG TCA ATG ATG G
Seq_W05F2 (-3.82)	TCC ACA AAA TGG CCT
Ch1-8.11(f23b5)_fwd	AGC GCT GCT CCG GTT CAT AGA TTG AGG ATC TGG AAC AGA AGT T
Ch1-8.11(f23b5)_rev	TGT GTG AGT CGC AAA CTC G
Ch1-8.11(f23b5)_seq	CGC AGT TTT TCA ATT TGT
Ch5amp50Left	AAA TTG CAC TTT GGG GGA TT
Ch5amp50Right	AGC GCT GCT CCG GTT CAT AGA TTG GGC GAT GAT GAA CAG AGA G
Ch5amp50Seq	TTT TCT TCA TTC TTT CCA

Appendix D continued

Primer Name	Sequence
Ch5amP56Left	AGC GCT GCT CCG GTT CAT AGA TTC CAA CAT TCT TGC ATG CCT A
Ch5amP56Right	GTG CTC GAT GAA GCG AAT TT
Ch5amP56Seq	TTC CTT GCT ATG TGA CTC T
5_C44B7 Ch 2 0.13	AGC GCT GCT CCG GTT CAT AGA TTC CGT GTA AAT GCT CAC CTC TGA CTC
3_C44B7 Ch 2 0.13	CAA CCC CAC TTC TTC AAA GTC TT
Seq_C44B7 Ch 2 0.13	AGT TGT TGG CGA CAG
5_W07E6 Ch 2 -15.87	AGC GCT GCT CCG GTT CAT AGA TTC TGT TCG ACA AAA AGC ACA C
3_W07E6 Ch 2 -15.87	TTT CGA ACA AAT TTT CAG ATC A
Seq_W07E6 Ch 2 -15.87	ATT CGT CAT ATA TTT TTT CT
5_F33E11 Ch5 amp56- Left	AGC GCT GCT CCGGTT CAT AGA TTC CAA CAT TCT TGC ATG CCT A
3_F33E11 Ch5 amp56- Right	GTG CTC GAT GAA GCG AAT TT
Seq_F33E11 Ch5 amp56- Seq	TTC CTT GCT ATG TGA CTC T
5_F49E2 Ch. X center	AGC GCT GCT CCG GTT CAT AGA TTC GCA ACT ATT GCC CAA AAC TGA G
3_F49E2 Ch. X center	TGC CAC GAG AGG TAT GGT AAT G
Seq_F49E2 Ch. X center	ATG CAC TTA GCC GGA
Chr5-2.37(c52a10)Fwd	AGC GCT GCT CCG GTT CAT AGA TTG GCC ATT TCA CAT TTT GGA TAA TCA
Chr5-2.37(c52a10)RE	AGC GCT GCT CCG GTT CAT AGA TT
Chr5-2.37(c52a10)SEQ	TCA ATC TTG AAA TAT CTT CC
Ch5-5.0(t28f12)Fwd	AGC GCT GCT CCG GTT CAT AGA TTG GGG TCA TTG ATG AGG GGT TA
Ch5-5.0(t28f12)Rev	AGC GCT GCT CCG GGT CAT AGA TT
Ch5-5.0(T28f12)Seq	GAT TTT GCG ATT TTC TGA
Ch5+1.11 (f20d6) Fwd	AGC GCT GCT CCG GTT CAT AGA TTC TTC TAT AGG TGC CA AAG GTG AG
Ch5+1.11 (f20d6) Rev	CCC TTC ACC GCA GTT GAC T
Ch5+1.11 (f20d6) Seq	GCA GTT GAC TTC GAA GC
Ch5+3.0(t19b10)Fwd	TCA AAG CTA CAG AAA ACC ACA CA
Ch5+3.0(t19b10)Rev	AGC GCTGCT CCG GTT CAT AGA TTA GCA CGA CAC TTT GCA TCT G
Ch5+3.0(t19b10)Seq	CAC AGA GAA AAT TAG GTG C
5_t28f12 Ch5	AGC GCT GCT CCG GTT CAT AGA TTG GTG TAG AGA GCT ACA CTC AGC
3_t28f12 Ch5	TTG GAT AGG CCT AGC AGA GC
Seq_t28f12 Ch5	GAT TTT GCG ATT TTC TGA A
5_f20d6 Ch5	AGC GCT GCT CCG GTT CAT AGA TTG CGA GGA ATG AGC AGT TCA GTA G
3_f20d6 Ch5	GAG AGT TCA CTG ACT ATG GC
Seq_f20d6 Ch5	GCA GTT GAC TTC GAA GC
5_c52a10 Ch5	AGC GCT GCT CCG GTT CAT AGA TTG TCT CGT GCC TTC CAT CCA AG
3_c52a10 Ch5	ATG GTC TCA GTT TAC CAG GAA G
Seq_c52a10 Ch5	TCA ATC TTG AAA TAT CTT CC
5_t19b10 Ch5	AGC GCT GCT CCG GTT CAT AGA TTG TAT TTC CCG CAA TGC TCT CC
3_t19b10 Ch5	CAA CCT ACT CTG CCT TTT GC
Seq_t19b10 Ch5	CAC AGA GAA AAT TAG GTG C
CHX(-1.89)B0403_fwd	TTG GCA GTC AAG AAT GTG TGG AGC GCT GCT CCG GTT CAT AGA TT
CHX(-1.89)B0403_rev	ATC GTT GCC TGG GCT TCA
CHX(-1.89)B0403_seq	AAC ATG CCA GCT CCA
CHX(+1.88)C32A9_fwd	TCA ATA TAA GAT TCA GGC GCT GTC AGC GCT GCT CCG GTT CAT AGA TT
CHX(+1.88)C32A9_rev	AAA GCA TTC CTA CCG TGT GTA AA
CHX(+1.88)C32A9_seq	GGA ATG TTC TGA AAA ATA AT
CHXFRC16H3_fwd	CGA TGC GGT TTC CTA GCT TAA GCG CTG GTC CGG TTC ATA GAT T
CHXFRC16H3_rev	CAT ATG GTC GCA AGA ACA GC
CHXFRC16H3_seq	CCA TCA TCT GAT ACA T

Appendix E: *them* mutants worms exhibit GaPP resistance in mCeHR-2 liquid media

N2 wild-type, IQ7280, IQ7310, IQ8280 and IQ9110 were grown in mCeHR-2 media supplemented with 0.05 μM , 0.1 μM , 0.5 μM and 2 μM GaPP. This experiment was conducted by Dr. Anita Rao.



Appendix F: List of primers used to clone missing constructs for GaPP RNAi screen

Primer Name	Sequence
5_W03D8.10	GGA GAT TCT CTC GGC TCT TC
5_W10C8.6_out	ATG ACT GTT GTC AAC GTT GAT AC
5_W10C8.6_in	TTT CTT GCC GCC TCT GGC GGT ATT CTT C
5_Y71F9AL.4	ACT TTC CCG CAA TAC GTG TAT G
5_Y71F9AR.3	GAA CAA CTA CCC CAA GCC TAC G
5_Y54E10A.11	GAC GAA AAA AGA CTG TCA GAC G
5_Y54E10A.17.2	GCA ACA CCC TCG TGG CTC
5_Y54E10A.14	GGT ACG TAT TGT CCA CAT TCG
5_Y47G6A.7b.2	GGA ATA TGT GCT TCA ATG GAT ATA G
5_Y71F9AM.6.1	CAC TCG CGG AGA ATA CAA CC
5_W03D8.8	ACT CTT TGA TTC ATC CGG AAC C
5_W03D8.9	GTC TCC GTC AAC GTG CCA C
5_W10C8.1	AAA TTC AAC TCG GAT TGG TGG
5_W03D8.11	ATT CCA GTC GAC GGT GAA AAG
5_K09H9.5	GCT TGT ATG GAG CAA GTA AAA TG
5_Y44E3B.2	ACT CGA ACT AGC GCT TCG
5_Y47G6A.19c	GCT CGA ATG TGG AGA AAA TC
5_Y47G6A.6	GTG GAC ATA TTC GGC GAG AAG
5_Y47G6A.12	GCG TTG CCG CTT GTT CG
5_Y54E10A.4b	GAT AGA GAT CAA GCC ATA CG
5_Y54E10BR.8	CAG TAC CAA TCC AAA CTG GAT G
5_Y54E10BR.3	GCT GCG GGT GGT GAA GG
5_Y71F9AL.17	GGA ACC ACT GAA GCT GCG
5_Y71F9B.13c	TTC GTC GCG GAC TGC AAT TTC
5_Y71F9AR.2	ATA TGC CGA AGG AAT TCT GG
5_Y71F9AL.9.2	TCA GTG CAC CAG CTC CAG C
5_Y71F9B.8	TGG CCA CCT TCG TCC AG
5_Y71F9AL.16	CGA TTC TGG AGA CGG AGT AAC
5_Y71F9B.7	ATT GAT GAT GCA GAA GCC GC

Appendix F continued

Primer Name	Sequence
3_W03D8.10	GAG AGC AGC CCC AAT TGC
3_W10C8.6_out	TTA AAT TCG GCG AGA GAG C
3_W10C8.6_in	CCG CCA GAG GCGG CAA GAA AAT GAG CAA AAT G
3_Y71F9AL.4	CTA TTC ACG CTT CTC AAT GTT CTC
3_Y71F9AR.3	CCG AAA AAG ATG AAT CTT CCC C
3_Y54E10A.11	CCT CCG AAG CAT CAT ATT CC
3_Y54E10A.17.2	TTA GTT AAA GAT CTT GCG GGT AC
3_Y54E10A.14	CAT CAG GAA TCT GCA TGC AAG
3_Y47G6A.7b.2	CCA ATT GAT CTC AGC TCC TTC
3_Y71F9AM.6.1	GTC AGC CTT CTT GGC GG
3_W03D8.8	TGC AAA ATA CTC CAT ATC TAC ATC
3_W03D8.9	CCA CCC AAG TAA GTG TAC GAG
3_W10C8.1	CCT CGA TCA TAG TCT CTA AGT C
3_W03D8.11	AAG CTC CAT TAA TTG CTC ATG
3_K09H9.5	TCA TAC AGA AAC AGG ACA TTC C
3_Y44E3B.2	CGA TAA TGG CAT GGT AGC CC
3_Y47G6A.19c	GGT TTC TTC AAT ATC TGG AGC
3_Y47G6A.6	CGG AAG CTG TGC TCC AAA TAG
3_Y47G6A.12	CCG AAT TCC TGT GCA TCA G
3_Y54E10A.4b	CGG TTC AGT TCC CAC ATC
3_Y54E10BR.8	CCT TAA GAT GCC GAA TAA CAT G
3_Y54E10BR.3	CCG TAC CTT TTT CAG ATG ATT C
3_Y71F9AL.17	CCC AGA CTG CTG GCT CG
3_Y71F9B.13c	CAA ATA CGC CTG GGG TCT C
3_Y71F9AR.2	CTG AAA AAT CGA GTG AAG ACC C
3_Y71F9AL.9.2	CTT TGT GTG TTG GGC TGA G
3_Y71F9B.8	CTT GTG ACT TTG GAA TCA AGT AG
3_Y71F9AL.16	CCG TCC ACC ACT CAG CG
3_Y71F9B.7	ATT GAA AAA GTT TAT CTG AAC AGT GCC

Appendix G: List of primers used to confirm mutations in *them* genomes

Primer Name	Sequence
5_Y39G10AR_RNAi	GAG AGC TCC ACG TAA GGA G
3_Y39G10AR_RNAi	CGA GCA ATC CTC AAG CGC
5_Y39G10AR_CST	TCT TCT TCT TCC CGC CGT C
3_Y39G10AR_CST	CTC GGC CAC CTT CAT AAC ATC
Y39G10AR_Seq_1	ATG GGA GAA CCT TCA CCT AG
Y39G10AR_Seq_2	CCA TGA AAA ATC GAT AAT TTC TAT C
Y39G10AR_Seq_3	GAA CAT TAA TCA ACA TTG GTA AC
Y39G10AR_Seq_4	CCA GCA GGG GTT ATA TCA G
Y39G10AR_Seq_5	GAG AAA AAA TAC CGG AAA ACG
5_F40E3.2_CST	GCA AAA GGT GTT CAA CAG GG
3_F40E3.2_CST	TAA TGT TTT TAT TCA TAA AAA AAA GAT ACT AGG
F40E3.2_Seq_1	CCC GAA TTC GAT CCT TTC G
F40E3.2_Seq_2	CTA CAT AGT TGT TCT TTA CAT TAA G
F40E3.2_Seq_3	GAA TTG TTA GCT GTT TCT GAT TCG
F40E3.2_Seq_4	CGC TTA CGA AAT CTA TTT TTG G
5_ftn1_CST	CAG GAT TGC AGT AGG CTT ATC
3_ftn1_CST	GAA CTT CAA ACA TGC AAA TTA ATC
ftn1_Seq_1	CCG AGG CGA CAA ATC CC
ftn1_Seq_2	CCA AAT AGC ATT GTA GGT AC
ftn1_Seq_3	GCT GAG GCA GAT AGA ATT GC
ftn1_Seq_4	CAA AAT GTA ATG TGA ATG TGG ACG
ftn1_Seq_5	GAT ATC GCA CTT CGG AAC ATT G
5_lin17_CST	CTT CAA CAC TCC CAT TAG TCC C
3_lin17_CST	CGC CCA CCT CTG CAT TAT TG
lin17_Seq_1	CCC ATG GAC CAC TTT CC
lin17_Seq_2	GAA TGG AGA ATG AGG GAA AAG
lin17_Seq_3	GGT TTT TGG CCA CAT TTT TAG TC
lin17_Seq_4	CTT CTT TCT GTG CTC TTC CC
lin17_Seq_5	GGG TAA TTT GAA ACG GGG G
lin17_Seq_6	CCA AGC CAA CCG GGT G
lin17_Seq_7	CTC TGA CAC CAC GAG ATT TG
lin17_Seq_8	GCT TTG CCG GTC AAA TAT AG
lin17_Seq_9	GGC CAC GTA GAA AAA TCA ATT AC
lin17_Seq_10	GAA CGA TTT TTG TGC GCT AAC
lin17_Seq_11	GAC GCG CAA AAT ATC TCG AAG
lin17_Seq_12	GAT TGG ATG GCC GAG TGG
lin17_Seq_13	GGA TCA AGT ACG GGG TTC
5_Y71F9AL.4_CST	CTC GTC GAA CTT CTC AGA AG
3_Y71F9AL.4_CST	AAA GAA CAT CGA GTG CCA TAT G
Y71F9AL.4_Seq_1	CCG AAT TTG CCG GAA ATT TTC
Y71F9AL.4_Seq_2	CCC ACA GGA AAG AAG AGG
Y71F9AL.4_Seq_3	GGG TTT TCA GAC AAT TTT GAG
Y71F9AL.4_Seq_4	CGA TTC GTG TGT ACG CAG
Y71F9AL.4_Seq_5	CAT TTT CCA GCC AAA AAT CGA G
Y71F9AL.4_Seq_6	GCT CCA TCG TAC AAA TCC AAT TG
5_Y47G6A.13_CST	GAA TCT GGA ACG ATA ATG ACG AC
3_Y47G6A.13_CST	AAT TCT TCG GGA GAA TGA TTT CAA G
Y47G6A.13_Seq_1	GTT TGA ATT ACC TCC AAA AGG
Y47G6A.13_Seq_2	GAT CTC TGA GTC TCA CCT C
Y47G6A.13_Seq_3	GGC ACT TCG CAT GAA GAT TC

Appendix G continued

Primer Name	Sequence
Y47G6A.13_Seq_4	CGG CAT TTT GAA CAT TTT GCA C
5_W03D8.5_CST	GTG CTG CAG GGA GAA GAT TC
3_W03D8.5_CST	GGC AAA TCG AGA AAC CGG C
W03D8.5_Seq_1	GGT AGT GGC AGC GGA G
W03D8.5_Seq_2	CTG GTC AAT TAC TCT TTA CAC C
5_K09H11.11_CST	GCG ATG GTA TGC TTG CTA CG
3_K09H11.11_CST	TCC ATC TTG CAA TCT TCC TAC AAA C
K09H11.11_Seq_1	GTG AAT GTT TCA GAG CAA ATC TC
K09H11.11_Seq_2	GAG GCC CCA CGA AAA GG
ttn1_Seq_1	TGA GAA AAT TGA TGT TGC CAC
ttn1_Seq_2	CTT TGG TCC AGC TGA CTT C
5_egl46_CST	TCA GTT CAC GCC AGA TGC AAG
3_egl46_CST	TGA TGC TTG AAG ATT CAA TAA AAA TTT ATT G
elg46_Seq_1	CGG GGC GGA GAC TCG
egl46_Seq_2	GAG TTT CTC CCA TTC CCC
egl46_Seq_3	GGT GAA ATA CGA GGA CGT G
egl46_Seq_4	GGC CAA TTT GGC ATC ACA TC
5_nhr147_CST	CAA CAA AGA ATG CAA AAA GAC ATG
3_nhr147_CST	TGC TGA TAT ACT CAT TAA CCA CTG
nhr147_Seq_1	GCA CAA GGA GAA GTC TGA TTC
nhr147_Seq_2	CAT CGG AAA GCA AAA AAG AAT TTA AC
nhr147_Seq_3	AGA TGC ATC ATT CTT TAT TGG C
3'W03D8.5 EXT1	TGT AAA TGG AAA AAC GTA TGC GCC
5'W03D8.5 FRAG1	GGA AGA ACA TGC GAC TTC CTT TTC C
3'W03D8.5 FRAG1	GGA AAA GGA AGT CGC ATG TTC TTC C
5'W03D8.5 FRAG2	CCG TCA TCG AGG TAG ACC ATG
3'W03D8.5 FRAG2	CAT GGT CTA CCT CGA TGA CGG
3'W03D8.5 EXT2	CAA ATC GCC GAG TTG GCG AAC
5'lin-17F1	CTC CTC GAG AGA CTG GCT C
3'lin-17F1	CTT TTC CCT CAT TCT CCA TTC C
5'lin-17F2	CCA GTG GAA GGG ATT TCT ATA C
3'lin-17F2	CCA CTT TTA CTA CGT GGC CG
5'lin-17F3	CGG GTA TTG TTT ACC CTT AAG ATT AAC
3'lin-17F3	TTG TAG GCA GGC AGG CAC C
5'lin-17F4	GGA CCT AAT GCA TCA GAT TTG ACG
3'lin-17F4	TCC CAA TTG CAA CCC TCT TTT CC
5'lin-17F5	GAA CAA ATT AGA GCA TAC TGC AAA TCC
3'lin-17F5	CTA ACA TGG TGC ATC GAT GTT AGC
5'lin-17F6	CCG CAT TTT TCG TAG ATC ACA CC
3'lin-17F6	CGT CAA ATG TGC TGT GCA ATA CG
5'lin-17F7	GCT TCC GTA ATG AAC CAA ACT TG
5'lin-17F7	CCC GTA AAT CAA AAG TAA AGA GAG
5'Y.13F1	ATG ACT AAT AGT GAT AAG TCT ACA TCG
3'Y.13F1	GCA CCA CGT GAT GAT GGC C
5'Y.13F2	CGC ATT TCC TCG TCC CTC G
3'Y.13F2	CAA AGA GAC TTT CTG ACA CCA TG
5'Y.13F3	CGG CAT TTT GAA CAT TTT GCA CAT TTA C
3'Y.13F3	AAC AGA CTC AAA ATG TGC TCA AAT TAA C
3'lin-17_INTR_1	GAG GAG TGG ACC CCA ACC
3'lin-17_INTR_2	CCG AAA TAC TTA AAA CTG TGC CG
3'lin-17_INTR_3	GCG TCT GAA AAT TGG TCT TTG CG

References

1. Andrews, N. C. (1999). Disorders of iron metabolism. *N Engl J Med*, 341: 1986-95.
2. (2003). Micronutrient deficiencies. Battling iron deficiency anaemia: The challenge. 2003. <http://www.who.int/nut/ida.htm>.
3. Ovesen, L., Bendtsen, F., Tage-Jensen, U., Pedersen, N., Gram, B., and Rune, S. (1986). Intraluminal pH in the stomach, duodenum, and proximal jejunum in normal subjects and patients with exocrine pancreatic insufficiency. *Gastroenterology*, 90: 958-62.
4. Spiro TG, B. G., Saltman P (1967). Hydrolytic polymerization of ferric citrate. II. Influence of excess citrate. *Journal of the American Chemical Society*, 89: 5559-5562.
5. Uzel, C., and Conrad, M. E. (1998). Absorption of heme iron. *Semin Hematol*, 35: 27-34.
6. Conrad, M. E., and Umbreit, J. N. (2000). Iron absorption and transport-an update. *Am J Hematol*, 64: 287-98.
7. Heinemann, I. U., Jahn, M., and Jahn, D. (2008). The biochemistry of heme biosynthesis. *Arch Biochem Biophys*, 474: 238-51.
8. Severance, S., and Hamza, I. (2009). Trafficking of heme and porphyrins in metazoa. *Chem Rev*, 109: 4596-616.
9. Tsiftoglou, A. S., Tsamadou, A. I., and Papadopoulou, L. C. (2006). Heme as key regulator of major mammalian cellular functions: Molecular, cellular, and pharmacological aspects. *Pharmacol. Ther.*, 111: 327-345.
10. Kresge, N., Simoni, R. D., and Hill, R. L. (2006). A pathway for heme biosynthesis: the work of David Shemin. *J. Biol. Chem.*, 281: 2.
11. Ajioka, R. S., Phillips, J. D., and Kushner, J. P. (2006). Biosynthesis of heme in mammals. *Biochim. Biophys. Acta*, 1763: 723-736.
12. Oliveira, M. F., Silva, J. R., Dansa-Petretski, M., de Souza, W., Lins, U., Braga, C. M., Masuda, H., and Oliveira, P. L. (1999). Haem detoxification by an insect. *Nature*, 400: 517-8.
13. Medlock, A. E., and Dailey, H. A. (2007) Regulation of mammalian heme biosynthesis. 116-127. Tetrapyrroles. Edited by Warren, M., and Smith, A. G., Landes Bioscience and Springer Science + Business Media, Austin
14. Rao, A. U., Carta, L. K., Lesuisse, E., and Hamza, I. (2005). Lack of heme synthesis in a free-living eukaryote. *Proc Natl Acad Sci U S A*, 102: 4270-5.
15. Chitwood, D. J. (2003). Research on plant-parasitic nematode biology conducted by the United States Department of Agriculture-Agricultural Research Service. *Pest Manage. Sci.*, 59: 748-753.
16. Stephenson, L. S., Latham, M. C., and Ottesen, E. A. (2000). Malnutrition and parasitic helminth infections. *Parasitology*, 121 Suppl: S23-38.
17. Fuller, V., Lilley, C., and Urwin, P. (2008). Nematode resistance. *New Phytol.*, 180: 27-44.
18. Shendure J, J. H. (2008). Next-generation DNA sequencing. *Nature Biotechnology*, 26: 1135-1145.

19. Shemin, D., and Rittenberg, D. (1945). THE UTILIZATION OF GLYCINE FOR THE SYNTHESIS OF A PORPHYRIN. *J. Biol. Chem.*, 159: 567-568.
20. Riddle, R., Yamamoto, M., and Engel, J. (1989). Expression of delta-aminolevulinate synthase in avian cells: separate genes encode erythroid-specific and nonspecific isozymes. *Proc. Natl. Acad. Sci. U.S.A.*, 86: 792-796.
21. Kaasik, K., and Lee, C. C. (2004). Reciprocal regulation of haem biosynthesis and the circadian clock in mammals. *Nature*, 430: 467-71.
22. Han L, L. J., Pan L, Wang X, Shao Y, Han S, Huang B (2006). Histone acetyltransferase p300 regulates the transcription of human erythroid-specific 5-aminolevulinate synthase gene. *Biochemical and Biophysical Research communications*, 348: 799-806.
23. Bevan DR, B. P., Shemin D (1980). Mechanisms of porphobilinogen synthase. Requirement of Zn²⁺ for enzyme activity. . *The Journal of Biological Chemistry*, 255: 2030-5.
24. Erskine, P. T., Senior, N., Awan, S., Lambert, R., Lewis, G., Tickle, I. J., Sarwar, M., Spencer, P., Thomas, P., Warren, M. J., Shoolingin-Jordan, P. M., Wood, S. P., and Cooper, J. B. (1997). X-ray structure of 5-aminolaevulinate dehydratase, a hybrid aldolase. *Nat. Struct. Mol. Biol.*, 4: 1025-1031.
25. Jaffe, E. K. (2003). An unusual phylogenetic variation in the metal ion binding sites of porphobilinogen synthase. *Chem Biol*, 10: 25-34.
26. Shoolingin-Jordan, P. M., Spencer, P., Sarwar, M., Erskine, P. E., Cheung, K. M., Cooper, J. B., and Norton, E. B. (2002). 5-Aminolaevulinic acid dehydratase: metals, mutants and mechanism. *Biochem. Soc. Trans.*, 30: 584-590.
27. Shoolingin-Jordan, P., Al-Dbass, A., McNeill, L., Sarwar, M., and Butler, D. (2003). Human porphobilinogen deaminase mutations in the investigation of the mechanism of dipyrromethane cofactor assembly and tetrapyrrole formation. *Biochem. Soc. Trans.*, 31: 731-5.
28. Krishnamurthy, P. C., Du, G., Fukuda, Y., Sun, D., Sampath, J., Mercer, K. E., Wang, J., Sosa-Pineda, B., Murti, K. G., and Schuetz, J. D. (2006). Identification of a mammalian mitochondrial porphyrin transporter. *Nature*, 443: 586-9.
29. Paterson, J. K., Shukla, S., Black, C. M., Tachiwada, T., Garfield, S., Wincovitch, S., Ernst, D. N., Agadir, A., Li, X., Ambudkar, S. V., Szakacs, G., Akiyama, S. I., and Gottesman, M. M. (2007). Human ABCB6 Localizes to Both the Outer Mitochondrial Membrane and the Plasma Membrane. *Biochemistry*, 46: 9443-9452.
30. Tsuchida, M., Emi, Y., Kida, Y., and Sakaguchi, M. (2008). Human ABC transporter isoform B6 (ABCB6) localizes primarily in the Golgi apparatus. *Biochem. Biophys. Res. Commun.*, 369: 369-375.
31. Grandchamp, B., Phung, N., and Nordmann, Y. (1978). The mitochondrial localization of coproporphyrinogen III oxidase. *Biochem. J.*, 176: 97-102.
32. Conder, L., Woodard, S., and Dailey, H. A. (1991). Multiple mechanisms for the regulation of haem synthesis during erythroid cell differentiation. Possible role for coproporphyrinogen oxidase. *Biochem. J.* , 275 (Pt 2): 321-326.
33. Koch, M., Breithaupt, C., Kiefersauer, R., Freigang, J., Huber, R., and Messerschmidt, A. (2004). Crystal structure of protoporphyrinogen IX oxidase: a key enzyme in haem and chlorophyll biosynthesis. *EMBO J.* , 23: 1720-1728.

34. Yin, L., Wu, N., Curtin, J. C., Qatanani, M., Szwegold, N. R., Reid, R. A., Waitt, G. M., Parks, D. J., Pearce, K. H., Wisely, G. B., and Lazar, M. A. (2007). Rev-erba, a Heme Sensor That Coordinates Metabolic and Circadian Pathways. *Science*, 318: 1786-1789.
35. Igarashi, K., and Sun, J. (2006). The heme-Bach1 pathway in the regulation of oxidative stress response and erythroid differentiation. *Antioxid Redox Signal*, 8: 107-18.
36. Rajagopal, A., Rao, A. U., Amigo, J., Tian, M., Upadhyay, S. K., Hall, C., Uhm, S., Mathew, M. K., Fleming, M. D., Paw, B. H., Krause, M., and Hamza, I. (2008). Haem homeostasis is regulated by the conserved and concerted functions of HRG-1 proteins. *Nature*, 453: 1127-31.
37. Tsiftoglou, A., Tsamadou, A., and Papadopoulou, L. (2006). Heme as key regulator of major mammalian cellular functions: molecular, cellular and pharmacological aspects. *Pharmacology & Therapeutics*, 111: 327-45.
38. Raghuram, S., Stayrook, K. R., Huang, P., Rogers, P. M., Nosie, A. K., McClure, D. B., Burris, L. L., Khorasanizadeh, S., Burris, T. P., and Rastinejad, F. (2007). Identification of heme as the ligand for the orphan nuclear receptors REV-ERB α and REV-ERB β . *Nat Struct Mol Biol*.
39. Beekvelt, M. V., Colier, W., Wevers, R., and Engelen, B. V. (2001). Performance of near-infrared spectroscopy in measuring local O₂ consumption and blood flow in skeletal muscle. *Journal of Applied Physiology*, 90: 511-519.
40. Yun, B., Matts, J., and Matts, R. (2005). Interdomain interactions regulate the activation of the heme-regulated eIF 2 alpha kinase. *Biochim Biophys Acta*, 1725: 174-81.
41. Tahara, T., Sun, J., Nakanishi, K., Yamamoto, M., Mori, H., Saito, T., Fujita, H., Igarashi, K., and Taketani, S. (2004). Heme positively regulates the expression of beta-globin at the locus control region via the transcriptional factor Bach1 in erythroid cells. *The Journal of Biological Chemistry*, 279: 5480-7.
42. Ogawa, K., Sun, J., Taketani, S., Nakajima, O., Nishitani, C., Sassa, S., Hayashi, N., Yamamoto, M., Shibahara, S., Fujita, H., and Igarashi, K. (2001). Heme mediates derepression of Maf recognition element through direct binding to transcription repressor Bach1. *Embo J*, 20: 2835-43.
43. Lipovich, L., Hughes, A. L., King, M. C., Abkowitz, J. L., and Quigley, J. G. (2002). Genomic structure and evolutionary context of the human feline leukemia virus subgroup C receptor (hFLVCR) gene: evidence for block duplications and de novo gene formation within duplicons of the hFLVCR locus. *Gene*, 286: 203-13.
44. Weiss, R. A., and Tailor, C. S. (1995). Retrovirus receptors. *Cell*, 82: 531-533.
45. Riedel, N., Hoover, E. A., Gasper, P. W., Nicolson, M. O., and Mullins, J. I. (1986). Molecular analysis and pathogenesis of the feline aplastic anemia retrovirus, feline leukemia virus C-Sarma. *J. Virol.*, 60: 242-250.
46. Quigley, J. G., Burns, C. C., Anderson, M. M., Lynch, E. D., Sabo, K. M., Overbaugh, J., and Abkowitz, J. L. (2000). Cloning of the cellular receptor for feline leukemia virus subgroup C (FeLV-C), a retrovirus that induces red cell aplasia. *Blood*, 95: 1093-9.

47. Quigley, J. G., Yang, Z., Worthington, M. T., Phillips, J. D., Sabo, K. M., Sabath, D. E., Berg, C. L., Sassa, S., Wood, B. L., and Abkowitz, J. L. (2004). Identification of a human heme exporter that is essential for erythropoiesis. *Cell*, 118: 757-66.
48. Keel, S. B., Doty, R. T., Yang, Z., Quigley, J. G., Chen, J., Knoblauch, S., Kingsley, P. D., De Domenico, I., Vaughn, M. B., Kaplan, J., Palis, J., and Abkowitz, J. L. (2008). A heme export protein is required for red blood cell differentiation and iron homeostasis. *Science*, 319: 825-8.
49. Krishnamurthy, P., and Schuetz, J. D. (2005). The ABC transporter Abcg2/Bcrp: role in hypoxia mediated survival. *Biometals*, 18: 349-58.
50. Jonker, J., Buitelaar, M., Wagenaar, E., van der Valk, M., Scheffer, G., Scheper, R., Plosch, T., Kuipers, F., Elferink, R., Rosing, H., Beijnen, J., and Schinkel, A. (2002). The breast cancer resistance protein protects against a major chlorophyll-derived dietary phototoxin and protoporphyria. *Proc. Natl. Acad. Sci. U.S.A.*, 99: 15649-54.
51. Krishnamurthy, P., Ross, D. D., Nakanishi, T., Bailey-Dell, K., Zhou, S., Mercer, K. E., Sarkadi, B., Sorrentino, B. P., and Schuetz, J. D. (2004). The stem cell marker Bcrp/ABCG2 enhances hypoxic cell survival through interactions with heme. *J Biol Chem*, 279: 24218-25.
52. Brenner, S. (1974). The genetics of *Caenorhabditis elegans*. *Genetics*, 77: 71-94.
53. Consortium, T. C. e. S. (1998). Genome Sequence of the Nematode *C. elegans*: A Platform for Investigating Biology. *Science*, 282: 2012-2018.
54. Kaletta T, H. M. (2006). Finding function in novel targets: *C. elegans* as a model organism. *Nature Reviews Drug Discovery*, 5: 387-399.
55. White, J. (1988) The nematode *C. elegans* (Wood, W. B., Ed.), Cold Spring Harbor Laboratory Press, New York
56. Jones, A., Buckingham, S., and Sattelle, D. (2005). Chemistry-to-gene screens in *Caenorhabditis elegans*. *Nature Reviews Drug Discovery*, 4: 321-30.
57. Riedl, C., and Sokolowski, M. (2004). Behavioral genetics: ganylyl cyclase prompts worms to party. *Current Biology*, 14: R657-8.
58. Moorman, C. (RH Plasterk). Functional characterization of the adenylyl cyclase gene *sgs-1* by analysis of a mutational spectrum in *Caenorhabditis elegans*. *Genetics*, 161: 133-42.
59. Kloek, A., McCarter, J., Setterquist, R., Schedl, T., and Goldberg, D. (1996). *Caenorhabditis* globin genes: rapid intronic divergence contrasts with conservation of silent exonic sites. *Journal of Molecular Evolution*, 43: 101-8.
60. Gotoh, O. (1998). Divergent structures of *Caenorhabditis elegans* cytochrome P450 genes suggest the frequent loss and gain of introns during the evolution of nematodes. *Molecular Biology and Evolution*, 15: 1447-59.
61. Colley, D. G., LoVerde, P. T., and Savioli, L. (2001). Infectious disease. Medical helminthology in the 21st century. *Science*, 293: 1437-1438.
62. Held, M. R., Bungiro, R. D., Harrison, L. M., Hamza, I., and Cappello, M. (2006). Dietary iron content mediates hookworm pathogenesis in vivo. *Infect Immun*, 74: 289-95.
63. Wu, B., Novelli, J., Foster, J., Vaisvila, R., Conway, L., Ingram, J., Ganatra, M., Rao, A. U., Hamza, I., and Slatko, B. (2009). The Heme Biosynthetic Pathway of

- the Obligate Wolbachia Endosymbiont of *Brugia malayi* as a Potential Antifilarial Drug Target. *PLoS Negl Trop Dis*, 3: e475.
64. Hoerauf, A., Volkmann, L., Nissen-Paehle, K., Schmetz, C., Autenrieth, I., Büttner, D., and Fleischer, B. (2000). Targeting of *Wolbachia endobacteria* in *Litomosoides sigmodontis*: comparison of tetracyclines with chloramphenicol, macrolides and ciprofloxacin. *Tropical Medicine & International Health*, 5: 275-279.
 65. Bruinsma, J., Schneider, D., Davis, D., and Kornfeld, K. (2008). Identification of mutations in *Caenorhabditis elegans* that cause resistance to high levels of dietary zinc and analysis using a genomewide map of single nucleotide polymorphisms scored by pyrosequencing. *Genetics*, 179: 811-28.
 66. Sanger, F., Air, G., Barrell, B., Brown, N., Coulson, A., Fiddes, C., Hutchison, C., Slocombe, P., and Smith, M. (1977). Nucleotide sequence of bacteriophage phi X174 DNA. *Nature*, 265: 687-95.
 67. Swerdlow, H., Wu, S. L., Harke, H., and Dovichi, N. J. (1990). Capillary gel electrophoresis for DNA sequencing. Laser-induced fluorescence detection with the sheath flow cuvette. *Journal of Chromatography*, 516: 61-67.
 68. Ewing, B., and Green, P. (1998). Base-calling of automated sequencer traces using phred. II. Error probabilities. *Genome Research*, 8: 186-94.
 69. Blazej, R., Kumaresan, P., and Mathies, R. (2006). Microfabricated bioprocessor for integrated nanoliter-scale Sanger DNA sequencing. *Proc Natl Acad Sci U S A*, 103: 7240-5.
 70. Gresham, D., Dunham, M., and Botstein, D. (2008). Comparing whole genomes using DNA microarray. *Nat Rev Genet*, 9: 291-302.
 71. Soni, G., and Meller, A. (2007). Progress toward ultrafast DNA sequencing using solid-state nanopores. *Clinical Chemistry*, 53: 1996-2001.
 72. Marguiles, M., Egholm, M., Altman, W., Attiya, S., Bade, J., Bemben, L., Berka, J., Braverman, M., Chen, Y., Chen, Z., Dewell, S., Du, L., Fierro, J., Gomes, X., Godwin, B., He, W., S, H., Ho, C., Irzyk, G., Jando, S., Alenquer, M., Jarvie, T., Jirage, K., and Kim, J. (2005). Genome Sequencing in microfabricated high-density picolitre reactors. *Nature*, 437: 376-80.
 73. Fedurco, M., Romieu, A., Williams, S., Lawrence, I., and Turcatti, G. (2006). BTA, a novel reagent for DNA attachment on glass and efficient generation of solid-phase amplified DNA colonies. *Nucleic Acids Res*, 34: e22.
 74. Turcatti, G., Romieu, A., Fedurco, M., and Tairi, A. (2008). A new class of cleavable fluorescent nucleotides: synthesis and optimization as reversible terminators for DNA sequencing by synthesis. *Nucleic Acids Res*, 36: e25.
 75. Nass, R., and Hamza, I. (2007) The nematode *C. elegans* as an animal model to explore toxicology in vivo: solid and axenic growth culture conditions and compound exposure parameters. 1.9.1-1.9.17. Current Protocols in Toxicology. Edited by Maines, M. D., Costa, L. G., Hodgson, E., Reed, D. J., and Sipes, I. G., John Wiley & Sons, Inc., New York
 76. Lyons, L., and Hcht, R. (1997). Acute ethanol exposure induces nondisjunction of the X chromosome during spermatogenesis. *Worm Breeders Gazette*, 14: 52.

77. Killian, D., and Hubbard, E. (2004). *C. elegans pro-1* activity is required for soma/germline interactions that influence proliferation and differentiation in the germ line. *Development*, 131: 1267-1278.
78. Wicks, S., Yeh, R., Gish, W., Waterson, R., and Plasterk, R. (2001). Rapid gene mapping in *Caenorhabditis elegans* using a high density polymorphism map. *Nature Genetics*, 28: 160-4.
79. Mello, C., Kramer, J., Stinchcomb, D., and Ambros, V. (1991). Efficient gene transfer in *C.elegans*: extrachromosomal maintenance and integration of transforming sequences. *EMBO J*, 10: 3959-70.
80. Kamath, R. S., and Ahringer, J. (2003). Genome-wide RNAi screening in *Caenorhabditis elegans*. *Methods*, 30: 313-21.
81. Barnhart, M., Pinkner, J., Soto, G., Sauer, F., Langermann, S., Waksman, G., Frieden, C., and Hultgren, S. (2000). PapD-like chaperones provide the missing information for folding of pilin proteins. *Proc. Natl. Acad. Sci.*, 97: 7709-14.